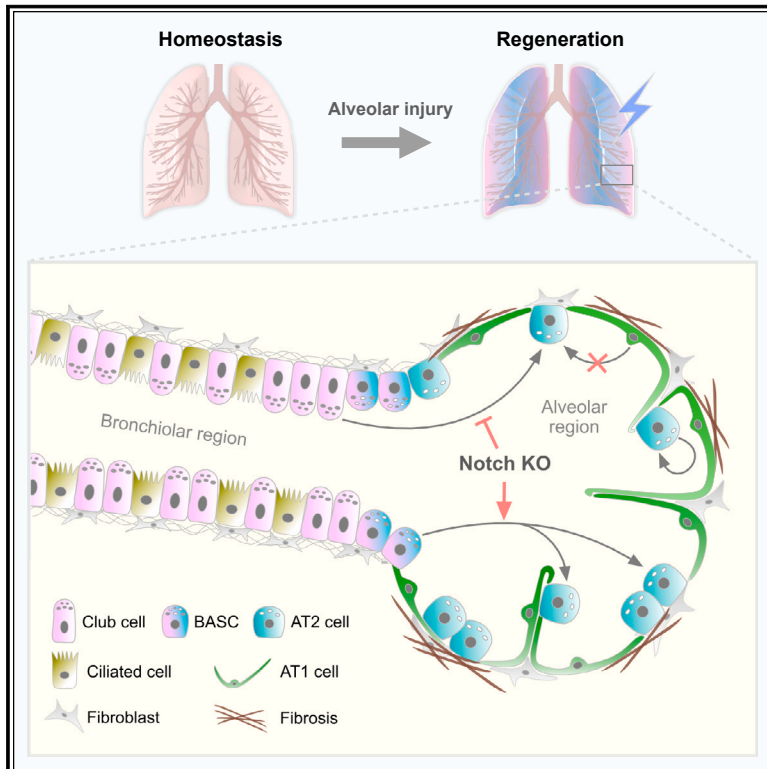


Tracing the origin of alveolar stem cells in lung repair and regeneration

Graphical abstract



Authors

Kuo Liu, Xinfeng Meng, Zixin Liu, ..., Wenjuan Pu, Huan Zhu, Bin Zhou

Correspondence

zhoubin@sibs.ac.cn

In brief

Using dual recombinase-mediated intersectional genetic approaches, Liu et al. find that alveolar stem cells (AT2 cells) are derived from existing AT2 cells, club cells, and BASCs but not from terminally differentiated AT1 cells during lung repair and regeneration.

Highlights

- AT1 cells do not contribute to AT2 cells during lung homeostasis and injury
- Intersectional genetics enables distinctive tracing of BASCs, club cells, and AT2 cells
- Club cells can contribute to the majority of alveoli after severe lung injuries
- Notch signaling distinctly regulates the cell fates of club cells and BASCs

Article

Tracing the origin of alveolar stem cells in lung repair and regeneration

Kuo Liu,^{1,2,4} Xinfeng Meng,^{3,4} Zixin Liu,^{2,4} Muxue Tang,² Zan Lv,² Xiuzhen Huang,² Hengwei Jin,² Ximeng Han,² Xiuxiu Liu,² Wenjuan Pu,² Huan Zhu,² and Bin Zhou^{1,2,3,5,*}

¹Key Laboratory of Systems Health Science of Zhejiang Province, School of Life Science, Hangzhou Institute for Advanced Study, University of Chinese Academy of Sciences, Hangzhou 310024, China

²New Cornerstone Investigator Institute, Key Laboratory of Multi-Cell Systems, Shanghai Institute of Biochemistry and Cell Biology, Center for Excellence in Molecular Cell Science, Chinese Academy of Sciences, University of Chinese Academy of Sciences, Shanghai 200031, China

³School of Life Science and Technology, ShanghaiTech University, Shanghai 201210, China

⁴These authors contributed equally

⁵Lead contact

*Correspondence: zhoubin@sibs.ac.cn

<https://doi.org/10.1016/j.cell.2024.03.010>

SUMMARY

Alveolar type 2 (AT2) cells are stem cells of the alveolar epithelia. Previous genetic lineage tracing studies reported multiple cellular origins for AT2 cells after injury. However, conventional lineage tracing based on Cre-loxP has the limitation of non-specific labeling. Here, we introduced a dual recombinase-mediated intersectional genetic lineage tracing approach, enabling precise investigation of AT2 cellular origins during lung homeostasis, injury, and repair. We found AT1 cells, being terminally differentiated, did not contribute to AT2 cells after lung injury and repair. Distinctive yet simultaneous labeling of club cells, bronchioalveolar stem cells (BASCs), and existing AT2 cells revealed the exact contribution of each to AT2 cells post-injury. Mechanistically, Notch signaling inhibition promotes BASCs but impairs club cells' ability to generate AT2 cells during lung repair. This intersectional genetic lineage tracing strategy with enhanced precision allowed us to elucidate the physiological role of various epithelial cell types in alveolar regeneration following injury.

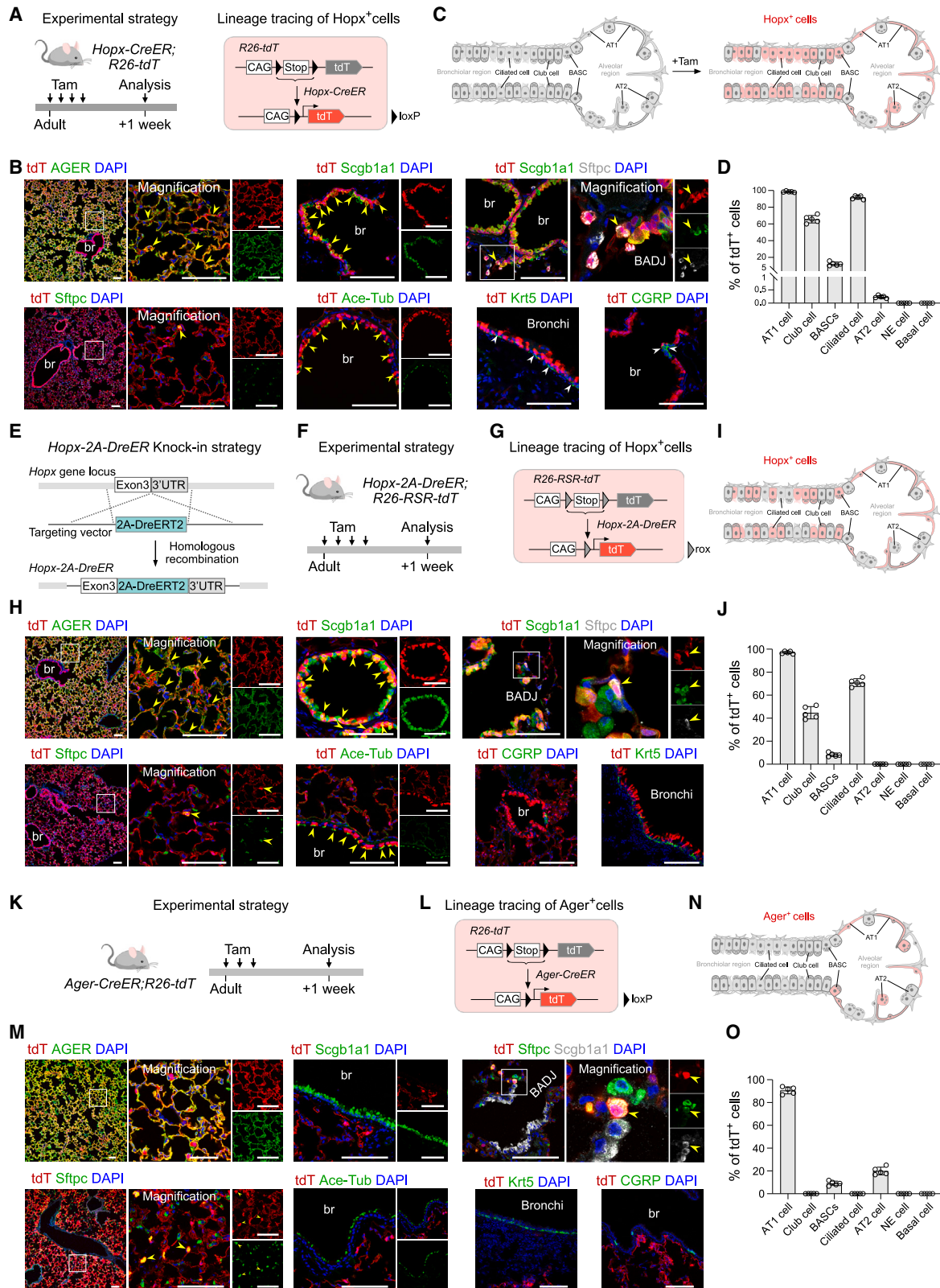
INTRODUCTION

Maintenance of the integrity of the alveolar structure and function is essential for proper lung homeostasis and function.¹ Structurally, the lung epithelium consists of the trachea, bronchioles, and alveolar regions. The identification of the molecular mechanisms by which lung epithelial stem/progenitor cells contribute to lung homeostasis provides invaluable insights into lung repair and regeneration after damage.^{1,2} Distinct stem/progenitor cell types reside in their local epithelial structure and are essential for maintenance and repair after lung injury.¹ Club cells and neuroendocrine cells have been identified as bronchiolar resident progenitors that are involved in bronchiolar regeneration after injury.^{3–5} The alveolar region is composed of alveolar type 1 (AT1) cells, which are responsible for gas exchange, and AT2 cells, which are considered to be stem cells capable of self-renewal and differentiation into AT1 cells during homeostasis and after injury.^{6–10} Additionally, a population of multipotent stem cells called bronchioalveolar stem cells (BASCs) was reported to exist at the bronchioalveolar-duct junction,¹¹ and they participate in the repair of bronchiolar and alveolar epithelium following lung injuries.^{11–14}

Multiple recent lineage tracing studies have proposed a new model that AT1 cells could also serve as a cellular origin for re-

generating alveolar epithelium after various alveolar injuries.^{15–21} Using the *Hopx-CreER* tool, Jain et al. reported that *Hopx*⁺ AT1 cells contribute to approximately 9% of AT2 cells in the lung following pneumonectomy (PNX) injury.¹⁵ Moreover, during hyperoxia-induced lung injury, *Hopx*⁺ AT1 cells were found to give rise to 10% and 30% of the renewed AT2 cells in adult and neonatal lungs, respectively.¹⁶ This key tool has also been used in a recent study to show that expression of KRAS(G12D) in differentiated AT1 cells reprograms them slowly and asynchronously back into AT2 stem cells, which in turn go on to generate indolent tumors.²² While the *Hopx* gene specifies AT1 progenitors around embryonic (E) day 13.5, *Hopx*⁺*Sftpc*⁺ bipotential progenitors continue to exist during prenatal and postnatal stages.^{23–25} Lineage tracing studies further showed that these bipotential progenitors can differentiate into both AT1 and AT2 cells during alveolar development.²⁴ Of note, a subset of AT2 cells was reported to be unexpectedly labeled by the *Hopx-CreER* tool.^{16,24} Therefore, it is crucial to re-evaluate the specificity of the *Hopx-CreER* tool and to elucidate the exact fate of AT1 cells during lung repair and tumor progression.

In addition to AT1 cells, *Scgb1a1*⁺ club cells have also been reported as progenitors for regenerating AT2 cells after bleomycin-induced lung injury.^{6,19–21} The H2–K1^{high} (MHC-I⁺) subset of club cells, identified through single-cell RNA-sequencing (scRNA-seq),



(legend on next page)

has been considered the primary progenitor of regenerating AT2 cells.^{19,21} Furthermore, genetic tracing of club cells using the *Scgb1a1-CreER* tool has indicated that club cells can migrate out of the bronchiolar region and regenerate alveolar epithelium after bleomycin injury.²⁰ However, controversy still exists due to the limitations of *in vitro* transplantation and non-specific genetic tracing *in vivo*. Previous studies have raised concerns about non-specific labeling by *Scgb1a1-CreER*, which ectopically labels a subset of AT2 cells and BASCs in addition to club cells.³ Considering that AT2 cells and BASCs are progenitors of new AT2 cells after injury, the non-specific labeling by *Scgb1a1-CreER* tool could strongly interfere with the interpretation of club cell fate. Therefore, controversies on the roles of AT1 cells and club cells exist regarding their exact contribution to AT2 cells during lung repair and regeneration. Thus, alternative genetic strategies are needed to specifically and simultaneously target these distinct cell populations. Here, we developed dual recombinase-mediated intersectional genetic strategies and conducted a comprehensive investigation into the cellular origins of AT2 cells during lung repair and regeneration.

RESULTS

Hopx-based genetic tools cannot specifically target AT1 cells

Previous studies reported that *Hopx*⁺ AT1 cells can de-differentiate into AT2 cells after lung injuries.^{15,16} To re-investigate the plasticity of *Hopx*⁺ cells during lung regeneration, we used the PNx and bleomycin models, as previously reported.^{6,15} We first conducted PNx-induced injury on adult *Hopx-CreER;R26-tdT* mice (Figure S1A).²⁶ Immunostaining data revealed that the proportion of *tdT*⁺*Sftpc*⁺ AT2 cells was significantly increased after PNx injury compared to the sham group (Figures S1B and S1C). Next, we used a bleomycin-induced acute alveolar injury model (Figure S1D). By immunostaining, we found that *Hopx*⁺ cells significantly contributed to 23.04 ± 2.32% of AT2 cells in damaged alveolar regions compared to the sham group (0.43 ± 0.08%) (Figures S1E and S1F). Of note, >80% of *tdT*⁺ AT2 cells were distributed within 400 μm from the bronchioles of bleomycin-injured *Hopx-CreER;R26-tdT* lungs (Figure S1G). Overall, the observation of *Hopx*⁺ cells de-differentiating into AT2 cells was consistent with previous reports.^{15,16,18}

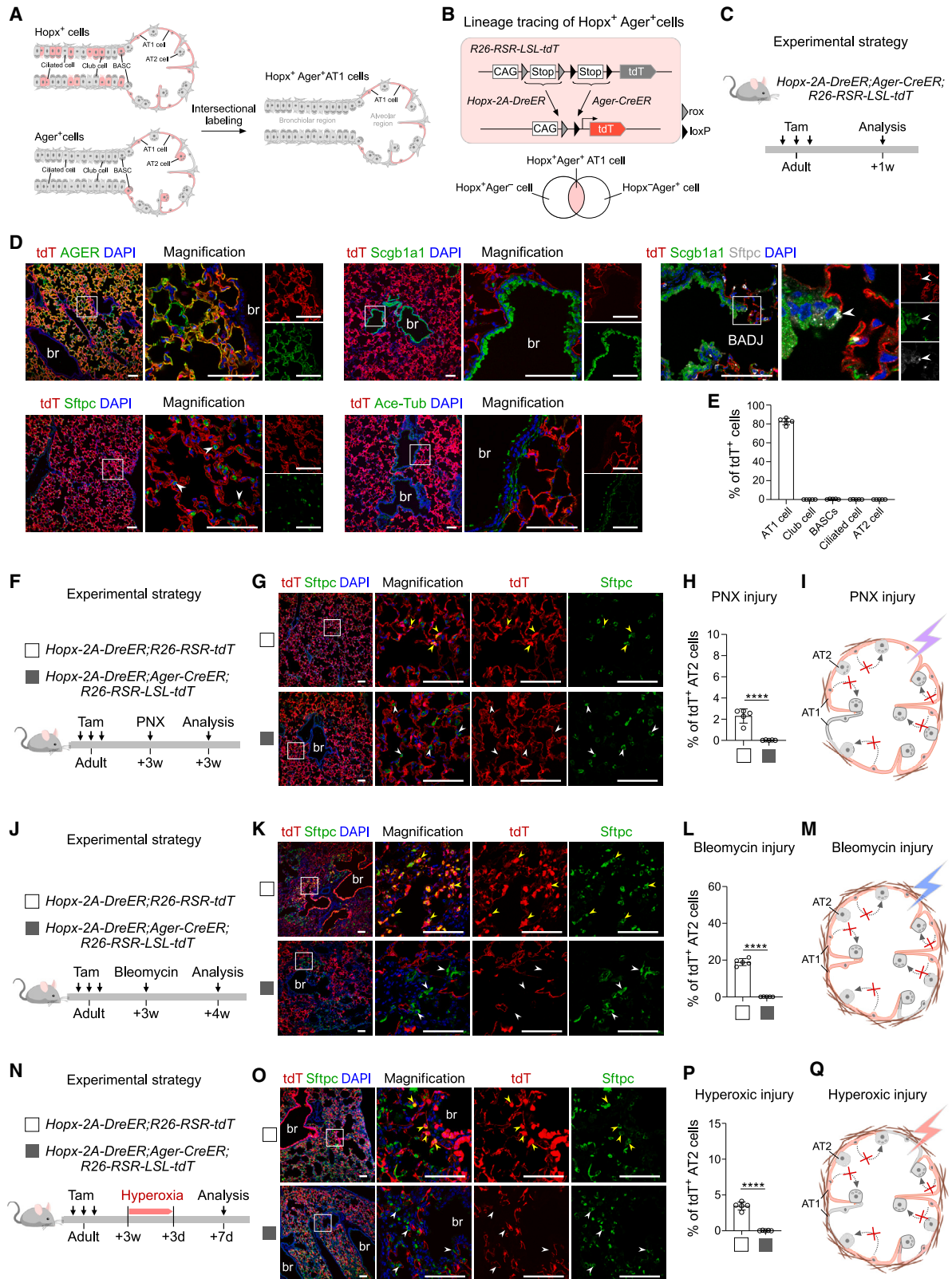
To examine the initial labeling profile of the *Hopx-CreER* tool, we collected the tissues of *Hopx-CreER;R26-tdT* mice within 3 days after tamoxifen (Tam) (Figure 1A). By immunostaining, we found that *tdT* was expressed in 98.50 ± 0.71% of *AGER*⁺ AT1 cells, 65.66 ± 4.45% of *Scgb1a1*⁺ club cells, 12.22 ± 2.24% of *Scgb1a1*⁺*Sftpc*⁺ BASCs, 91.65 ± 2.08% of *Acetylated-tubulin (Ace-Tub)*⁺ ciliated cells, and 0.24 ± 0.05% of *Sftpc*⁺ AT2 cells, but not in neuroendocrine (NE) and basal cells, indicating the *Hopx* is not only a marker for AT1 cells but also expressed in other types of epithelial cells (Figures 1B–1D). Therefore, the *Hopx*-based genetic tool ectopically labeled a subset of BASCs, club cells, and AT2 cells, which were reported to be progenitors for regenerating AT2 cells after alveolar injury (Figure S1H). Moreover, *Hopx-CreER* also labeled basal cells in the trachea (Figures S1I–S1K). We also found that *Hopx-CreER* is not a specific genetic tool for targeting the AT1 cells at prenatal and postnatal stages (Figures S1L–S1V).

To rule out the possibility that the broad labeling could be due to gene haploinsufficiency in *Hopx-CreER* mice, we generated a *Hopx-2A-DreER* line by inserting the 2A-DreER after the endogenous *Hopx* gene (Figure 1E).²⁷ Like the Cre-loxP system, Dre is another site-specific recombinase, and rox is its recognition site.²⁸ We crossed *Hopx-2A-DreER* mice with corresponding reporter *R26-RSR-tdT* mice²⁹ to trace *Hopx*⁺ cells (Figures 1F and 1G). We found that 97.08 ± 1.04% of AT1 cells, 44.78 ± 5.36% of club cells, 8.22 ± 1.59% of BASCs, 70.92 ± 3.35% of ciliated cells, and 0.14 ± 0.04% of AT2 cells were labeled by *tdT* in adult mice (Figures 1H–1J). Moreover, non-specific labeling was also observed at prenatal and neonatal stages in *Hopx-2A-DreER;R26-RSR-tdT* mice (Figures S2A–S2F), confirming that genetic tools based on *Hopx* are not specific for AT1 cells.

Given this limitation, we used a third mouse line with a different gene promoter, *Ager-CreER*,³⁰ to target AT1 cells (Figures 1K and 1L). We found that *tdT* was detected in 90.64 ± 3.05% of AT1 cells, 19.92 ± 3.35% of AT2 cells, and 9.10 ± 1.94% of BASCs but not in club, ciliated, basal, or NE cells in adult *Ager-CreER;R26-tdT* mice after Tam (Figures 1M–1O). Similar labeling patterns were observed at prenatal and postnatal stages of *Ager-CreER;R26-tdT* mice (Figures S2G–S2L). Collectively, the above results indicate that *Hopx*- and *Ager*-based genetic tools are not specific for tracing AT1 cells.

Figure 1. *Hopx*- or *Ager*-based genetic tools are not specific for labeling AT1 cells

- (A) A schematic diagram illustrating the experimental design.
(B) Immunostaining of *tdT*, *AGER*, *Scgb1a1*, *Sftpc*, *Ace-Tub*, *Krt5*, and *CGRP* on lung sections.
(C) Cartoon image showing labeled pulmonary cells in *Hopx-CreER;R26-tdT* mice.
(D) Quantification of the percentage of AT1, club, BASCs, ciliated, AT2, basal, and NE cells that were labeled by *tdT* in (B).
(E) A schematic diagram illustrating generation of *Hopx-2A-DreER* line.
(F and G) A schematic diagram illustrating the experimental design.
(H) Immunostaining of *tdT*, *AGER*, *Scgb1a1*, *Sftpc*, *Ace-Tub*, *Krt5*, and *CGRP* on lung sections.
(I) Cartoon image showing labeled pulmonary cells in *Hopx-2A-DreER;R26-RSR-tdT* mice.
(J) Quantification of the percentage of AT1, club, BASCs, ciliated, AT2, basal, and NE cells labeled by *tdT* in (H).
(K and L) A schematic diagram illustrating the experimental design.
(M) Immunostaining of *tdT*, *AGER*, *Scgb1a1*, *Sftpc*, *Ace-Tub*, *Krt5*, and *CGRP* on lung sections.
(N) Cartoon image showing labeled pulmonary cells in *Ager-CreER;R26-tdT* mice.
(O) Quantification of the percentage of AT1, club, BASCs, ciliated, AT2, basal, and NE cells labeled by *tdT* in (M).
Data are mean ± SD; *n* = 5. Scale bars, 100 μm.



(legend on next page)

Hopx⁺Ager⁺ AT1 cells do not de-differentiate into AT2 cells after lung injury

While the genetic tools based on *Ager* and *Hopx* were not specific to AT1 cells (Figures 1I and 1N), their ectopic labeling of lung epithelial cells was almost mutually exclusive; thus, their intersectional labeling could be highly restricted to AT1 cells (Figure 2A). To test this hypothesis, we employed the dual recombinase-mediated intersectional genetic reporter, *R26-RSR-LSL-tdT*,³¹ to label Hopx⁺Ager⁺ AT1 cells using *Hopx-2A-DreER* and *Ager-CreER* lines (Figure 2B). After Dre-rox and Cre-loxP recombinations, the tdT reporter gene is activated to label Hopx⁺Ager⁺ cells (Figure 2B). We then generated *Hopx-2A-DreER;Ager-CreER;R26-RSR-LSL-tdT* triple positive mice to characterize this strategy (Figure 2C). Immunostaining showed that tdT was expressed in $83.03 \pm 4.23\%$ of AT1 cells, $0.04 \pm 0.03\%$ of club cells, $0.41 \pm 0.37\%$ of BASCs, $0.04 \pm 0.02\%$ of AT2 cells, and $0.05 \pm 0.03\%$ of ciliated cells (Figures 2D and 2E), indicating that the labeling of AT1 cells was highly specific using this strategy.

We then examined the plasticity of AT1 cells after lung injury. We first performed PNx-induced injury and analyzed the lungs after 3 weeks (3w), with *Hopx-2A-DreER;R26-RSR-tdT* mice used as the control (Figure 2F). Immunostaining showed the presence of tdT⁺ AT2 cells in the control mice, whereas tdT⁺ AT2 cells were not detected in the triple positive mice, indicating that AT1 cells did not de-differentiate into AT2 cells after PNx (Figures 2G–2I). Next, we performed bleomycin-induced injury to determine the plasticity of AT1 cells in acute alveolar injury (Figure 2J). By immunostaining, we detected a subset of tdT⁺ AT2 cells in the control mice but no tdT⁺ AT2 cells in the triple positive mice (Figures 2K–3M, S3A, and S3B). We found that tdT⁺ basal-like cells and transitional AT2 cells could be detected in the control mice but not in the triple positive mice after bleomycin injury (Figure S3C). Additionally, we also investigated the plasticity of AT1 cells under conditions of hyperoxia-induced lung injury (Figure 2N). We found tdT⁺ AT2 cells in the control mice but not in the triple positive mice, indicating that AT1 cells did not de-differentiate into AT2 cells after hyperoxic injury (Figures 2O–2Q). Collectively, these data showed that Hopx⁺Ager⁺ AT1 cells are terminally differentiated cells and

cannot de-differentiate into AT2 cells at sites of lung injury in the PNx, bleomycin, or hyperoxia models.

Hopx⁺ AT1 cells lack cell plasticity to generate AT2 cells after lung injury

Given that the labeled Hopx⁺Ager⁺ AT1 cell subpopulation (~80%) constitutes a part of AT1 cells, we next aimed to explore the plasticity of the entire Hopx⁺ AT1 cell population. Considering that *Hopx-2A-DreER* targeted “unwanted” club cells, ciliated cells, BASCs, and AT2 cells, we then employed an alternative dual recombinases-responding reporter, nested reporter 2 (*R26-NR2*),²⁸ to specifically target the Hopx⁺ AT1 cells (Figure 3A). In *R26-NR2* design, Dre-rox recombination leads to ZsGreen (ZsG) expression in Dre⁺ cells, while Cre-loxP recombination removes the ZsG gene and Stop sequence and leads to tdT expression in both Dre⁺Cre⁺ and Dre⁻Cre⁺ cells (Figure 3A). Based on this design, we used *Hopx-2A-DreER* to label all potential Hopx⁺ AT1 cells and employed *Sox2-CreER* and *Sftpc-CreER* to block the labeling of “unwanted” Hopx⁺Sox2⁺ club cells and ciliated cells, as well as “unwanted” Hopx⁺Sftpc⁺ AT2 cells and BASCs, respectively (Figure 3A). We then generated *Hopx-2A-DreER;Sox2-CreER;Sftpc-CreER;R26-NR2* quadruple knockin mice, with *Hopx-2A-DreER;R26-NR2* mice serving as the control (Figure 3B). We found that $97.81 \pm 0.44\%$ of AT1 cells, $67.62 \pm 4.03\%$ of ciliated cells, $37.69 \pm 2.74\%$ of club cells, and $0.19 \pm 0.04\%$ of AT2 cells expressed ZsG in the control mice, consistent with the labeling observed in *Hopx-CreER;R26-tdT* and *Hopx-2A-DreER;R26-RSR-tdT* mice (Figures 3C–3E and S3D–S3H). In the quadruple knockin mice, $97.82 \pm 0.70\%$ of AT1 cells were labeled by ZsG, and virtually all the ectopically labeled cells detected in the control mice were now converted to tdT labeling, including ciliated cells, club cells, BASCs, and AT2 cells (Figures 3C–3E and S3I). These data demonstrate that the nested reporter system can specifically target AT1 cells, with higher labeling efficiency (Figure 3D) compared to the intersectional genetic strategy (Figure 2E).

We next investigated the plasticity of these AT1 cells after lung injury induced by PNx (Figure 3F). By immunostaining, we found that ZsG⁺ AT2 cells were detected in the control mice after PNx-induced injury (Figures 3G and 3H), but not in the quadruple

Figure 2. Intersectional genetics reveal that AT1 cells do not contribute to AT2 cells

- (A) A cartoon image showing the intersectional genetic strategy for lineage tracing of Hopx⁺Ager⁺ AT1 cells.
(B) A schematic diagram showing the lineage tracing strategy.
(C) A schematic diagram illustrating the experimental design.
(D) Immunostaining of tdT, AGER, Scgb1a1, Sftpc, and Ace-Tub on lung sections.
(E) Quantification of the percentage of AT1, club, BASCs, ciliated, and AT2 cells that were labeled by tdT in (D).
(F) A schematic diagram illustrating the experimental design.
(G) Immunostaining of tdT and Sftpc on lung sections after PNx injury.
(H) Quantification of the percentage of Sftpc⁺ AT2 cells expressing tdT in (G). *****p* < 0.0001.
(I) A cartoon image showing that AT1 cells do not contribute to AT2 cells in the PNx-induced injury.
(J) A schematic diagram illustrating the experimental design.
(K) Immunostaining of tdT and Sftpc on lung sections after bleomycin injury.
(L) Quantification of the percentage of Sftpc⁺ AT2 cells labeled by tdT in (K). *****p* < 0.0001.
(M) A cartoon image showing that AT1 cells do not regenerate AT2 cells in bleomycin-induced injury.
(N) A schematic diagram illustrating the experimental design.
(O) Immunostaining of tdT and Sftpc on lung sections after hyperoxia injury.
(P) Quantification of the percentage of Sftpc⁺ AT2 cells labeled by tdT in (O). *****p* < 0.0001.
(Q) A cartoon image showing that AT1 cells do not regenerate AT2 cells in hyperoxia-induced injury.
Data are mean ± SD; *n* = 5. Scale bars, 100 μm.

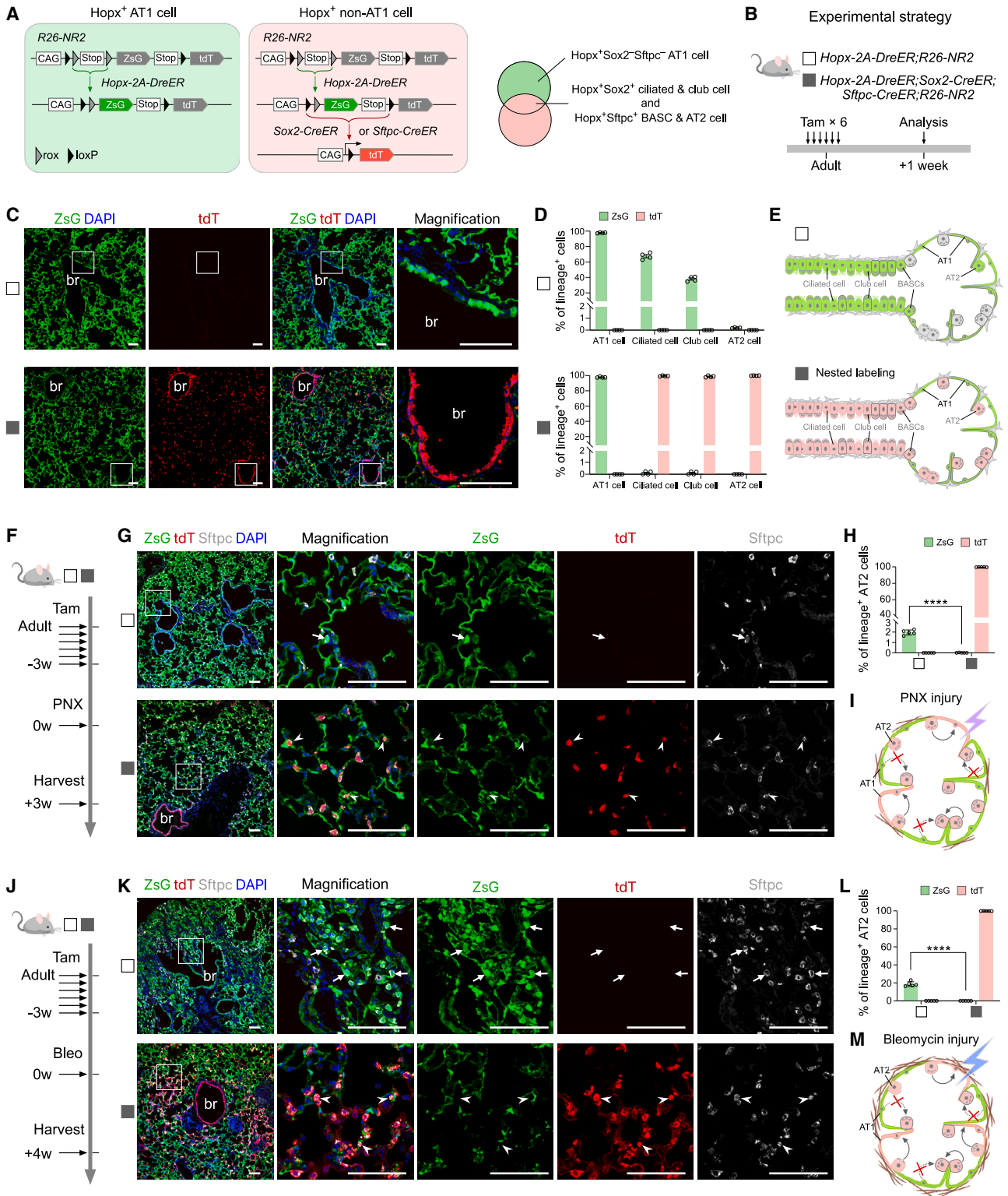


Figure 3. Hopx⁺ AT1 cells lack cell plasticity to generate AT2 cells after lung injury

(A) A schematic diagram illustrating the nested genetic strategy.

(B) A schematic diagram illustrating the experimental design.

(C) Immunostaining of ZsG and tdT on lung sections.

(legend continued on next page)

knockin mice, whereas AT2 cells were labeled by tdT (Figures 3G and 3H), suggesting that AT1 cells did not give rise to AT2 cells in this injury model (Figure 3I). We also collected the lungs at 4w after bleomycin treatment (Figure 3J). By immunostaining, we observed the presence of a subset of ZsG⁺ AT2 cells distributed near the bronchiolar region in the control mice after injury (Figures 3K and 3L), but we did not detect any ZsG⁺ AT2 cells in both the alveolar and peribronchiolar regions in the quadruple knockin mice (Figures 3K and 3L). These data indicate that AT1 cells were highly specialized and incapable of de-differentiating into AT2 cells after bleomycin-induced alveolar injury (Figure 3M).

Intersectional genetics distinguishes the contribution of club cells and BASCs to alveolar regeneration

Our data showed that the vast majority of *Hopx-CreER*-derived AT2 cells after bleomycin injury were distributed around the bronchioles (Figures S1G and S1H). We hypothesized that the *Hopx*⁺ cell-derived AT2 cells may originate from the other ectopically labeled cells, such as club cells or BASCs. We then designed a new intersectional genetic tracing strategy by generating *Hopx-2A-DreER;Scgb1a1-CreER;R26-RSR-LSL-tdT* triple positive mice, which enables simultaneous labeling of *Hopx*⁺ club cells and BASCs (Figures S4A–S4C). By immunostaining of lung sections after bleomycin injury, we found that the tdT⁺ cells differentiated into *Sftpc*⁺ AT2 and *AGER*⁺ AT1 cells after lung injury but not in the vehicle group (Figures S4D and S4E). These data showed that *Hopx*⁺*Scgb1a1*⁺ cells could contribute to AT2 cells, consistent with recent studies reporting that club cells, based on the *Scgb1a1* genetic tool, can contribute to AT2 cells.^{19–21} However, as the *Hopx*⁺*Scgb1a1*⁺ cells or *Scgb1a1*⁺ cells^{19–21} contain both club cells and BASCs, these previous genetic tracing data could not distinguish the cell origins for AT2 cells. *Scgb1a1-CreER* was not a specific tool for labeling club cells, as it also targeted BASCs and very few AT2 cells, in addition to club cells (Figures S4F–S4I). Therefore, genetic lineage tracing studies based on the *Scgb1a1* tool encountered the same caveat as the *Hopx*-based tool.

Due to the lack of exclusive club-cell-specific genetic tools, we then used another intersectional reporter, *R26-TLR*,³² to distinctly label club cells, BASCs, and AT2 cells. By design, *Dre*⁺*Cre*⁻ cells are labeled with ZsG after *Dre-rox* recombination, *Dre*⁻*Cre*⁺ cells are labeled with tdT after *Cre-loxP* recombination, and *Dre*⁺*Cre*⁺ cells are labeled with ZsG and tdT after both *Dre-rox* and *Cre-loxP* recombinations, resulting in a fluorescent yellow color (Figure 4A). The Stop sequences of *R26-tdT* and *R26-TLR* were about 900 base pairs (bp) and 1,730 bp, respec-

tively. We found that the longer Stop sequence of *Scgb1a1-CreER;R26-TLR* mice reduced the baseline labeling of club cells and ectopic labeling of AT2 cells compared to *Scgb1a1-CreER;R26-tdT* mice (Figures S4F–S4I).

BASCs have the properties of expressing both the club cell gene marker *Scgb1a1* and the AT2 cell gene marker *Sftpc*. To distinguish the labeling of club cells, BASCs, and AT2 cells, we generated *Scgb1a1-CreER;Sftpc-DreER;R26-TLR* triple positive mice (Figures 4A and 4B), in which *Scgb1a1*⁺ club cells are labeled with tdT (Club-tracer), *Sftpc*⁺ AT2 cells are labeled with ZsG (AT2-tracer), and *Scgb1a1*⁺*Sftpc*⁺ BASCs are labeled with tdT and ZsG (BASC-tracer). We collected the lungs to characterize the labeling of cells by this strategy after Tam (Figure 4C). By immunostaining, we found specific labeling of *Scgb1a1*⁺*Sftpc*⁻ club cells with tdT, *Sftpc*⁺ AT2 cells with ZsG, and *Scgb1a1*⁺*Sftpc*⁺ BASCs with tdT and ZsG (Figure 4D). Thus, this intersectional genetic strategy enabled us to distinguish three distinct progenitors and examine their cell fates with unique genetic reporters simultaneously in the same mice.

Next, we explored the cellular plasticity of these cell types after lung injury. We first performed PNX injury (Figure 4E). By immunostaining, we found that the Club-tracer did not contribute to AT2 cells in the sham mice, and it minimally contributed to AT2 cells in the peribronchiolar region after injury (Figures 4F and 4G). Similarly, the BASC-tracer contributed minimally to AT2 cells around the bronchioalveolar-duct junctions (BADJs) after injury (Figures 4F and 4G). The majority of AT2 cells were labeled by the AT2-tracer, suggesting that AT2 cells acted as the dominant progenitors for regenerating alveolar epithelium in PNX-injured lungs (Figure 4G).

We then investigated the cell plasticity of these cell types during bleomycin-induced lung injury (Figure 4H). By immunostaining, we found that a large proportion of AT2 cells adjacent to bronchioles were labeled with either tdT⁺ZsG⁻ or tdT⁺ZsG⁺ after injury, indicating that these AT2 cells were derived distinctively from the Club-tracer and the BASC-tracer, respectively (Figure 4I). Quantification data showed that club cells, BASCs, and AT2 cells contributed to 26.51 ± 7.24%, 11.39 ± 3.31%, and 60.41 ± 5.92% of AT2 cells, respectively, in the damaged alveolar region after injury (Figure 4J). We then evaluated whether alveolar expansion of club cells represents repair or bronchiolization. Immunostaining for tdT, ZsG, *Sftpc*, *Lamp3*, *AGER*, *Krt5*, *Scgb1a1*, or *Ace-Tub* on lung sections at 4w after bleomycin injury showed that, among the Club-tracer-derived alveolar cells, 58.73 ± 5.75% were *Sftpc*⁺ AT2 cells, 15.35 ± 2.22% were *AGER*⁺ AT1 cells, 3.34 ± 0.89% were *Krt5*⁺ basal-like cells, 3.84 ± 1.65% were *Scgb1a1*⁺ club-like cells, and none were

(D) Quantification of the percentage of AT1, ciliated, club, and AT2 cells labeled by ZsG and tdT. Data are mean ± SD; n = 4.

(E) A cartoon image showing cell labeling by different strategies.

(F) A schematic diagram illustrating the experimental design.

(G) Immunostaining for ZsG, tdT, and *Sftpc* on lung sections.

(H) Quantification of the percentage of *Sftpc*⁺ AT2 cells expressing ZsG or tdT in (G). ****p < 0.0001. n = 5.

(I) A cartoon image showing that the *Hopx*⁺ AT1 cells do not transdifferentiate to AT2 cells after PNX injury.

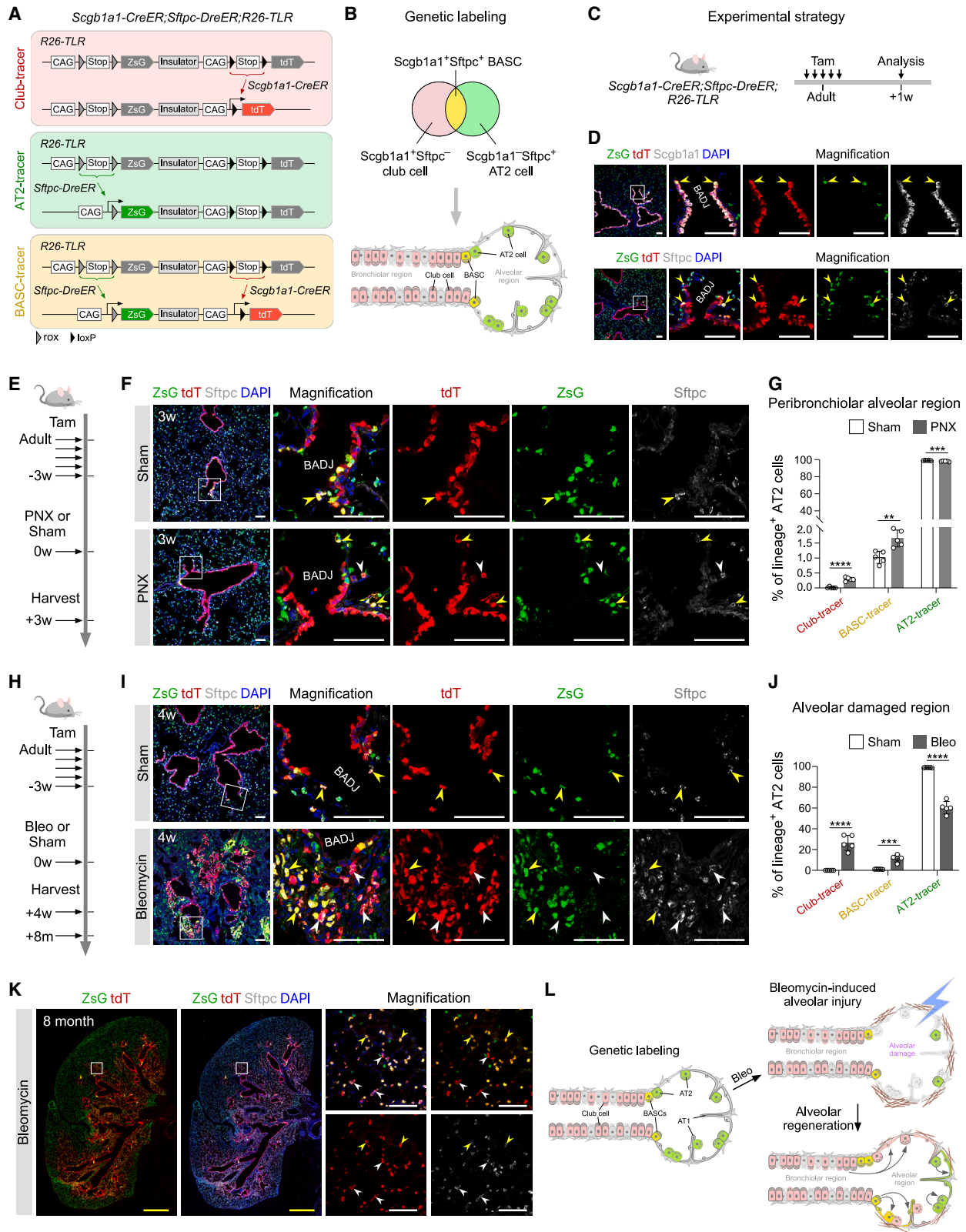
(J) A schematic diagram illustrating the experimental design.

(K) Immunostaining of ZsG, tdT, and *Sftpc* on lung sections after bleomycin injury.

(L) Quantification of the percentage of *Sftpc*⁺ AT2 cells expressing ZsG or tdT in (K). ****p < 0.0001. n = 5.

(M) A cartoon image showing that the *Hopx*⁺ AT1 cells do not transdifferentiate to AT2 cells.

Data are mean ± SD. Scale bars, 100 μm.



(legend on next page)

Ace-Tub⁺ ciliated-like cells (Figures S4J–S4L). The proportion of alveolar epithelial cells (AT2 and AT1) accounted for more than 70%, suggesting that the majority of alveolar expansion of Club-tracer represents repair after alveolar injury (Figure S4L).

Furthermore, we collected lungs at 8 months (m) to investigate the cell fates at the long-term regeneration stage (Figure 4H). By immunostaining, we found that both the AT2 cells derived from the Club-tracer and the BASC-tracer were expanded further from the bronchioles at 8m compared to the 4w short-term regeneration time point (Figure 4K). Taken together, we found that club cells can respond to alveolar injuries and contribute AT2 and AT1 cells to regenerate the alveolar epithelium (Figure 4L).

Club cells have the potential to generate the majority of the alveoli after injuries

We next asked to what extent could club cells contribute to alveolar stem cells after alveolar injury. We hypothesized that club cells may exhibit more plasticity when the regenerative ability of AT2 cells and BASCs are sequestered after lung injury. To this end, we generated an alveolar injury model by combining p21 overexpression in BASCs and AT2 cells with bleomycin-induced injury (bleomycin & p21-OE). The p21 protein is a cell-cycle inhibitor that can inhibit cell proliferation.^{33,34} We showed that the proliferation of p21-AT2 cells was significantly inhibited compared to the sham group after bleomycin injury (Figures S4M–S4O). Noticeably, overexpression of p21 in AT2 cells promoted their differentiation into AT1 cells (Figures S4N and S4P), consistent with previous reports.^{20,21,35}

We next generated *Sftpc-DreER;R26-rox-p21-GFP;Scgb1a1-CreER;R26-LZL-tdT* quadruple knockin mice (p21 genetic model) to investigate the potential of club cells to regenerate alveoli after bleomycin injury (Figure 5A).³⁶ In this design, *Scgb1a1*⁺ club cells are labeled as tdT after Cre-loxP recombination (Club-tracer2), *Sftpc*⁺ AT2 cells are labeled as green fluorescent protein (GFP) and p21 after Dre-rox recombination (AT2-tracer2), and *Scgb1a1*⁺*Sftpc*⁺ BASCs are labeled as tdT, GFP, and p21 after both Cre-loxP and Dre-rox recombinations (BASC-tracer2) in the quadruple knockin mice (Figures 5A and 5B). After bleomycin injury, the contribution of AT2 cells and BASCs to lung regeneration is impaired due to the inhibition of cell proliferation, enabling us to investigate the potential of only club cells during repair (Figure 5B). We first collected lung sam-

ples at 1w and 8w for analysis after Tam without injury (Figure 5C). By immunostaining, we found that club cells, AT2 cells, and BASCs were tdT⁺, GFP⁺, and GFP⁺tdT⁺, respectively, at 1w, indicating distinctive genetic labeling of these three progenitor cell populations (Figure 5D). Notably, in the 8w lungs, we detected a few tdT⁺*Sftpc*⁺*GFP*⁻*Scgb1a1*⁻ AT2 cells distributed around BADJs (Figures 5D and 5E).

We next induced bleomycin-mediated injury to investigate the plasticity of club cells during lung repair (Figure 5F). By immunostaining and quantification of lung sections at 4w after injury, we found that at the damaged region, 47.32 ± 6.88% of AT2 cells were derived from club cells, while the contribution of the BASC-tracer2 and AT2-tracer2 was significantly decreased compared to that in the sham mice (Figures 5G and 5H). Immunostaining and its quantification showed that among Club-tracer2-derived alveolar cells, 64.30 ± 4.92% were *Sftpc*⁺ AT2 cells, 23.31 ± 4.56% were *AGER*⁺ AT1 cells, 3.99 ± 1.55% were *Krt5*⁺ basal-like cells, 3.72 ± 1.76% were *Scgb1a1*⁺ club-like cells, and none were Ace-Tub⁺ ciliated-like cells (Figures 5I, 5J, S5A, and S5B). The proportion of alveolar epithelial cells (AT2 and AT1) accounts for more than 80%, which also represents a broad alveolar repair program after injury (Figure S5B).

Although we found part of the club-derived alveolar cells expressing Sox2, most of these tdT⁺Sox2⁺ cells also expressed mature AT2 or AT1 cell markers (Figures S5C–S5F). The proportion of alveolar epithelium contributed by the club cells (~47%) in the context of p21-overexpression was higher than that in the non-p21 strategy (Figure 4J, ~27%), indicating that impaired proliferation of AT2 cells promotes club cell-mediated repair and regeneration of the alveoli.

To explore the role of club cells in long-term repair, we collected lungs at 8m (after bleomycin injury for analysis (Figure 5F)). We detected a tremendous number of tdT⁺ cells that spread to the far edges of the lung and occupied the entire injured area in some lung lobes during long-term repair (Figure 5K). By immunostaining, we found that there was differentiation of club cells into AT2 cells or AT1 cells, and in some severely injured lung lobes, club cells contributed to virtually all AT2 cells (Figures 5L and 5M). Quantification of all lung lobes showed that the percentage of club-cell-derived AT2 cells increased to 81.87 ± 4.33% at 8m, while the percentage of AT2 cells derived from AT2 cells and BASCs decreased to less than 20% combined compared to those in the sham group

Figure 4. Distinctly labeled club cells and BASCs contribute to alveolar epithelium after lung injury

(A and B) A schematic diagram illustrating the intersectional genetic strategy.

(C) A schematic diagram illustrating the experimental design.

(D) Immunostaining of ZsG, tdT, *Scgb1a1*, or *Sftpc* on lung sections after Tam.

(E) A schematic diagram illustrating the experimental design.

(F) Immunostaining of ZsG, tdT, and *Sftpc* on lung sections.

(G) Quantification of the percentage of *Sftpc*⁺ AT2 cells that were labeled by Club-tracer, BASC-tracer, and AT2-tracer after PNx injury in (F). *****p* < 0.0001; ***p* = 0.0037; ****p* = 0.0005.

(H) A schematic diagram illustrating the experimental design.

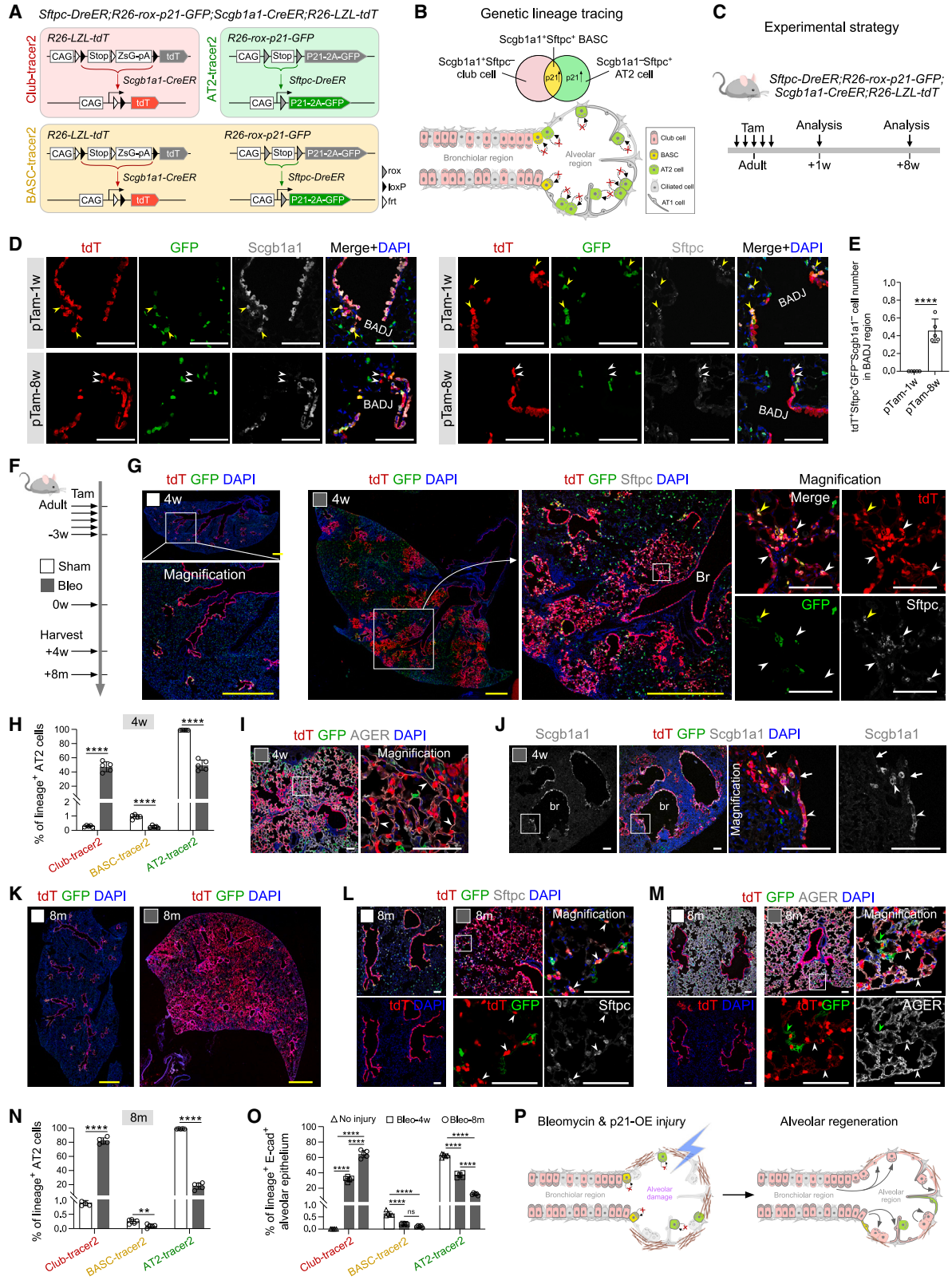
(I) Immunostaining of ZsG, tdT, and *Sftpc* on lung sections after bleomycin injury.

(J) Quantification of the percentage of *Sftpc*⁺ AT2 cells that were labeled by Club-tracer, BASC-tracer, and AT2-tracer after bleomycin injury in (I). *****p* < 0.0001; ****p* = 0.0001.

(K) Immunostaining of ZsG, tdT, and *Sftpc* on lung sections.

(L) A cartoon image showing that club cells and BASCs could regenerate AT2 cells.

Data are mean ± SD; *n* = 5. Yellow bars, 1mm; white bars, 100 μm.



(legend on next page)

(Figure 5N). Additionally, the contribution of these three progenitors to the total E-cad⁺ alveolar epithelium showed a similar trend at different injury time points (Figure 5O). Compared with the sham group, the cell death of GFP⁺ AT2 cells was significantly increased after injury (Figures S5G and S5H). Taken together, these data indicate that club cells exhibit a high degree of cellular plasticity and have a great potential to regenerate the vast area of impaired alveoli at the sites of bleomycin & p21-OE-induced injury (Figure 5P).

To confirm the large potential of club cells to generate alveoli, we utilized another genetic strategy (a diphtheria toxin [DT]-based genetic model) to induce alveolar damage. We generated *Sftpc-mGFP-DTR* line by knocking a mGFP (membrane GFP)—P2A—diphtheria toxin receptor (DTR) cassette into the endogenous *Sftpc* gene locus (Figure S5I). In these mice, all *Sftpc*⁺ cells, including *Sftpc*⁺ BASCs and *Sftpc*⁺ AT2 cells, could be deleted after DT treatment. Immunostaining of lung sections showed that virtually all *Sftpc*⁺ AT2 cells expressed GFP and DTR in the vehicle group, whereas after DT treatment, hardly any signals for GFP, DTR, or *Sftpc* could be detected (Figure S5J). Next, we designed a *Sftpc-mGFP-DTR;Scgb1a1-CreER;R26-LZL-tdT* triple positive mice to allow for specific depletion of the *Sftpc*⁺ BASCs and *Sftpc*⁺ AT2 cells by DT treatment and simultaneous tracing of the *Scgb1a1*⁺ club cells (Club-tracer3, Figure S5K). By immunostaining, we found that club cells, AT2 cells, and BASCs were specifically labeled by tdT, GFP, and both tdT and GFP, respectively, after Tam (Figures S5L and S5M). Club cells contributed to 66.18 ± 5.99% of AT2 cells in DT-inhaled lobes at 6w post-DT injury (Figures S5N–S5P). Immunostaining revealed that among Club-tracer3-derived alveolar cells, 71.23 ± 2.92% were *Sftpc*⁺ AT2 cells, 17.96 ± 2.17% were AGER⁺ AT1 cells, 2.78 ± 0.53% were Krt5⁺ basal-like cells, 2.46 ± 0.63% were *Scgb1a1*⁺ club-like cells, and none were Ace-Tub⁺ ciliated-like cells (Figures S5Q and S5R). The proportion of alveolar epithelial cells (AT2 and AT1) accounts for ~90%, suggesting the great potential of club cells for regenerating alveoli after injury.

Heterogeneity in the conversion of club cells and BASCs to alveoli

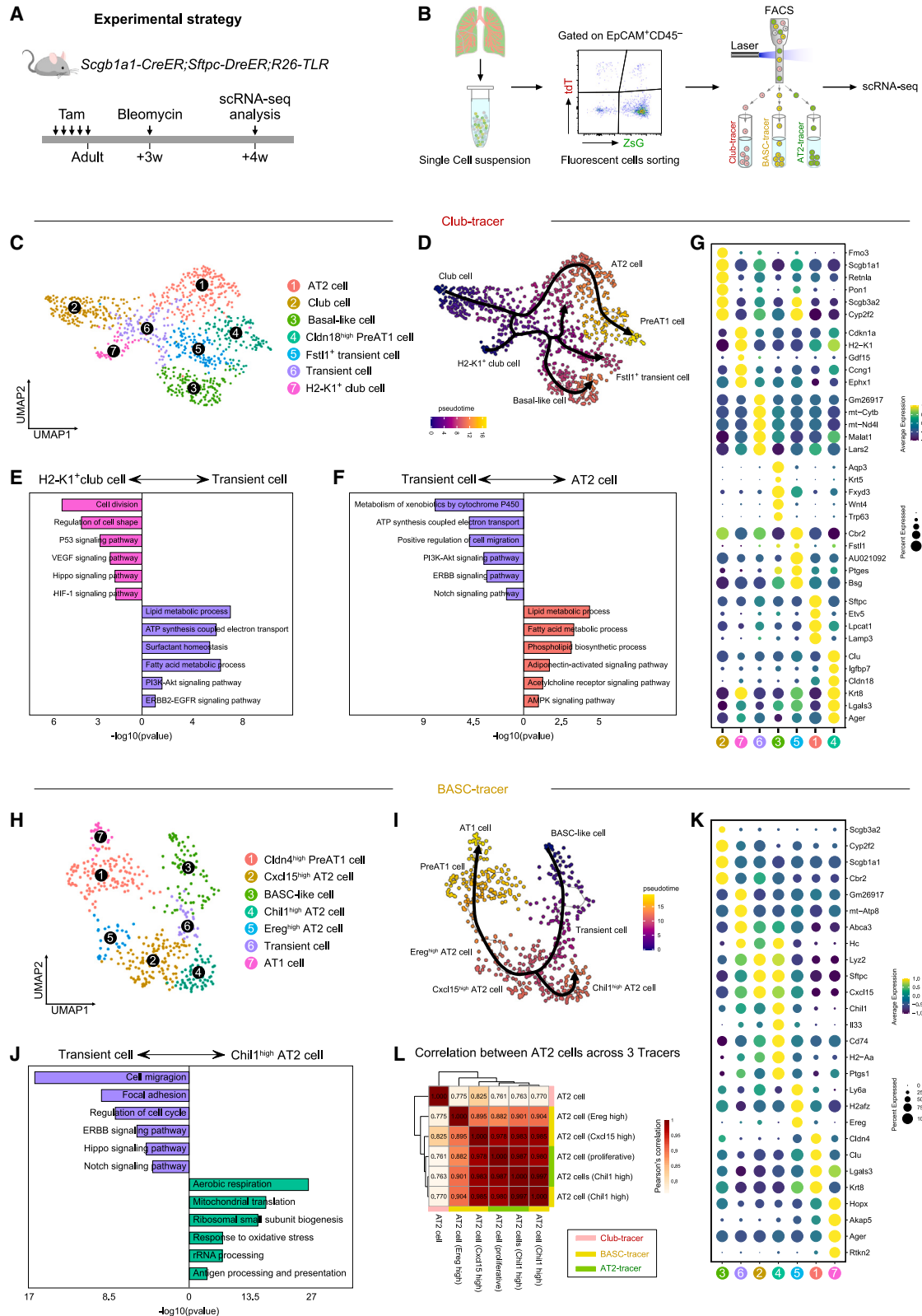
To further understand their dynamic contribution to alveolar regeneration, we performed scRNA-seq of cells separated by

Club-tracer (tdT⁺ZsG⁻), BASC-tracer (tdT⁺ZsG⁺), and AT2-tracer (tdT⁺ZsG⁺) from *Scgb1a1-CreER;Sftpc-DreER;R26-TLR* mice after bleomycin injury (Figures 6A and 6B). As self-renewal of AT2 cells has been well studied, we were therefore interested in studying club-cell-to-AT2-cell and BASCs-to-AT2-cell conversions. With UMAP analysis, we identified 7 cell clusters for the Club-tracer, each with distinctive key markers (Figures 6C–6G). We identified the club cells (cluster 2) by their expression of canonical club cell markers (*Scgb1a1*, *Scgb3a2*, and *Cyp2f2*) and also identified a subset of club cells (cluster 7) that also exhibited high expression of *H2-K1*, which was consistent with a previous report.¹⁹ The AT2 cell cluster (cluster 1) was identified by its expression of canonical AT2 cell markers (*Sftpc*, *Etv5*, and *Lamp3*). Cluster 6 was identified by expression of *Gm26917*, *mt-Cytb*, *mt-Nd4l*, *Malat1*, and *Lars2*. We also identified another *Fstl1*⁺ transient cell cluster (cluster 5) with increased expression of the AT2 cell marker *Cbr2* and the fibrosis-related gene *Fstl1*.³⁵ Moreover, a basal-like cluster (cluster 3) was marked by high expression of *Trp63* and *Krt5*. The pre-AT1 cell cluster (cluster 4) was identified by increased expression of a AT1 cell marker (*Ager*) and high expression of *Cldn18* and the inter-mediated cell marker *Krt8*.²¹ By immunofluorescence staining of representative markers for Club-tracer cell clusters, we also characterize their spatial location *in vivo* (Figures S6A–S6C).

We then investigated the connections between the clusters of the Club-tracer. Pseudotime trajectory plotting revealed that the fate transition initiated from both club cells and *H2-K1*⁺ club cells and then entered the transient state (Figure 6D). Subsequently, the transient cells could differentiate directly to AT2 cells or to AT2 cells via the *Fstl1*⁺ transient state, which was consistent with our *in vivo* fate mapping data. We then compared the transcription profiles between the *H2-K1*⁺ cell cluster and the transient cluster. Gene ontology (GO) analysis showed that the *H2-K1*⁺ cell cluster was highly enriched in gene pathways of cell division and regulation of cell shape as well as the p53, VEGF, Hippo, and HIF-1 signaling pathways (Figure 6E). The transient cell cluster increased the expression of genes related to surfactant homeostasis, lipid metabolism, and ATP synthesis (Figure 6E). Further analysis and comparison of the enriched genes between the transient cell cluster and AT2 cell cluster showed that the transient cells were highly enriched in genes

Figure 5. Club cells can regenerate the majority of the alveoli after lung injury

- (A) A schematic diagram illustrating the genetic lineage tracing strategy.
 (B) A schematic diagram illustrating the club, AT2, and BASCs were specifically labeled in the quadruple knockin line in (A).
 (C) A schematic diagram illustrating the experimental design.
 (D) Immunostaining of tdT, GFP, *Scgb1a1*, or *Sftpc* on lung sections.
 (E) Quantification of the number of *Sftpc*⁺ AT2 cells labeled by Club-tracer2 in (D). *****p* < 0.0001.
 (F) A schematic diagram illustrating the experimental design.
 (G) Immunostaining of tdT, GFP, and *Sftpc* on lung sections.
 (H) Quantification of the percentage of *Sftpc*⁺ AT2 cells that were labeled by Club-tracer2, BASC-tracer2, and AT2-tracer2. *****p* < 0.0001.
 (I) Immunostaining of tdT, GFP, and AGER on lung sections.
 (J) Immunostaining of tdT, GFP, and *Scgb1a1* on lung sections.
 (K) Immunostaining of tdT and GFP on lung sections.
 (L) Immunostaining of tdT, GFP, and *Sftpc* on lung sections.
 (M) Immunostaining of tdT, GFP, and AGER on lung sections.
 (N and O) Quantification of the percentage of *Sftpc*⁺ AT2 cells (N) or E-cad⁺ alveolar cells (O) that were labeled by Club-tracer2, BASC-tracer2, and AT2-tracer2 after sham or bleomycin treatment. *****p* < 0.0001; ***p* = 0.0079.
 (P) Cartoon image showing the contribution of club cells to alveolar regeneration.
 Data are mean ± SD; *n* = 5 mice. Yellow bars, 1mm; white bars, 100 μm.



(legend on next page)

related to cell migration and Notch signaling, and the AT2 cells were more enriched in genes related to lipid and fatty acid metabolism and the phospholipid biosynthetic process (Figure 6F).

For the BASC-to-AT2-cell conversion, UMAP analysis revealed 7 cell clusters for cells from the BASC-tracer (Figures 6H–6K). The BASC-like cluster (cluster 3) was identified by its enrichment of club cell marker genes (*Scgb1a1* and *Cyp2f2*) and an AT2 cell marker (*Cbr2*). A transient cell cluster (cluster 6) exhibited low club cell marker expression and increased expression of marker genes, including *Gm26917*, *mt-Atp8*, *Abca3*, and *Hc* (Figures 6H and 6K). Moreover, we identified three subpopulations of AT2 cell clusters (*Cxcl15*^{high} AT2 cluster 2, *Chil1*^{high} AT2 cluster 4, and *Ereg*^{high} AT2 cluster 5) and two subpopulations of AT1 cell clusters (*Cldn4*^{high} PreAT1 cluster 1 and AT1 cluster 7) (Figure 6H). Furthermore, by pseudotime trajectory analysis, we found that BASCs converted into *Cxcl15*^{high} AT2 cells via a transient cell state and then proceeded into two differentiation routes: *Chil1*^{high} cluster 4 and *Ereg*^{high} cluster 5, which led to further AT1 differentiation (cluster 1 to 7) (Figure 6I). We then compared the enriched genes between the transient cell cluster and *Chil1*^{high} AT2 cluster. GO analysis revealed that the former cluster was highly enriched in cell migration, cell cycle, focal adhesion and Notch signaling, while the latter cluster was highly enriched for genes related to mitochondrial translation, rRNA processing, and antigen processing and presentation (Figure 6J). By immunofluorescence staining of representative markers for BASC-tracer cell clusters, we characterize their spatial location *in vivo* (Figures S6B–S6D).

We then compared the Club-tracer and BASC-tracer and observed that the basal-like cell and *Fstl1*⁺ transient cell were cell populations detected exclusively in the Club-tracer, both of which exhibited their unique characteristics in gene expression (Figures S7A and S7B). A comparison of our dataset with club cells and BASCs at homeostasis¹² showed that many pathways were altered in club cells and BASCs after bleomycin injury (Figures S7C–S7G).

We also compared the correlation between the lineage-labeled AT2 cells from Club-tracer, BASC-tracer, and AT2-tracer. AT2 cells from the AT2-tracer were identified as two clusters: proliferative AT2 cell cluster and *Chil1*^{high} AT2 cell cluster. By comparison, we found that AT2-tracer-derived AT2 cells had the highest correlation with the BASC-tracer-derived *Chil1*^{high} AT2 cells, followed by *Cxcl15*^{high} AT2 cells, *Ereg*^{high} AT2 cells, and then Club-tracer-derived AT2 cells (Figures 6L and S7H–S7J). Notably, AT2 cells of the Club-tracer showed a high degree of correlation with those of the BASC-tracer, while within the

BASCs-tracer, the AT2 cell populations exhibited a more pronounced correlation among themselves (Figure 6L). Collectively, our data showed that both similarities and differences existed between club-derived alveolar cells and BASC-derived alveolar cells, and the conversion of club cells and BASCs to AT2 cells involved two different processes with distinct differentiation programs.

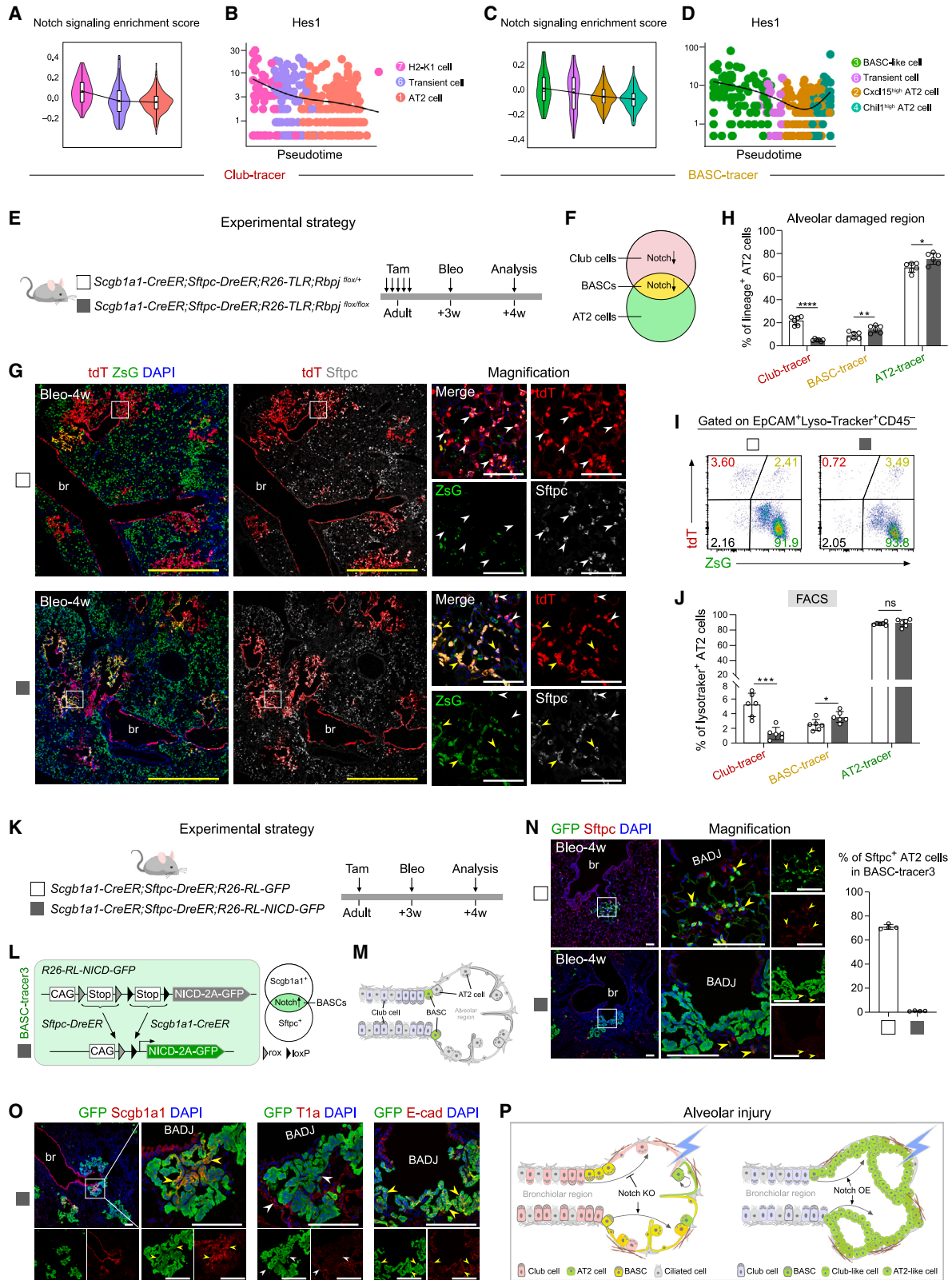
Notch distinctly regulates the conversion of club cells and BASCs into AT2 cells

Our findings revealed enrichment of Notch signaling in the transient cell state during AT2 differentiation for both the Club-tracer and the BASC-tracer (Figures 6F and 6J). We further found that in both the Club-tracer and the BASC-tracer, the gene expression levels of Notch signaling and its downstream key factor, *Hes1*, were downregulated during AT2 cell differentiation, suggesting a potential regulatory role of Notch signaling in the transition (Figures 7A–7D).

To examine the function of the Notch signaling in club cells and BASCs during alveolar repair, we generated *Scgb1a1-CreER;Sftpc-DreER;R26-TLR;Rbpj*^{fllox/fllox} (mutant group) and *Scgb1a1-CreER;Sftpc-DreER;R26-TLR;Rbpj*^{fllox/+} (control group) mice for simultaneous tracing and knockdown of the Notch signaling in cells from the Club-tracer and the BASC-tracer (Figures 7E and 7F). By immunostaining, we found that club cells and BASCs contributed to AT2 cells in both mutant and control mice after injury (Figure 7G). However, the percentage of Club-tracer-derived AT2 cells was significantly lower in the mutant ($5.02 \pm 0.92\%$) compared to that in the control ($21.77 \pm 3.69\%$) post-injury (Figures 7G and 7H). In contrast, the percentage of BASC-tracer-derived AT2 cells was significantly greater in the mutant ($14.51 \pm 3.16\%$) compared to that in the control ($8.93 \pm 2.88\%$) after injury (Figure 7H). The percentage of AT2-tracer-derived AT2 cells was significantly higher in the mutant ($75.60 \pm 4.90\%$) compared to that in the control ($67.90 \pm 4.04\%$) after injury (Figure 7H). Moreover, compared to the control group, the percentage of Club-tracer-derived tdT⁺E-cad⁺ alveolar area was significantly decreased in the mutant group, while the percentage of BASC-tracer-derived tdT⁺ZsG⁺E-cad⁺ alveolar area was significantly increased in the mutant group (Figure S7K). Flow cytometric analysis of AT2 cells (EpCAM⁺Lysotracker⁺CD45⁺) revealed opposite trends in the sources of AT2 cells derived from the Club-tracer (mutant, $1.30 \pm 0.84\%$ versus control, $5.19 \pm 1.61\%$) and the BASC-tracer (mutant, $3.55 \pm 0.75\%$ versus control $2.47 \pm 0.75\%$) after bleomycin-induced

Figure 6. Heterogeneity in the conversion of Club cells and BASCs into alveolar epithelium

- (A) A schematic diagram illustrating the experimental design.
- (B) A cartoon image showing the strategy for cell sorting and scRNA-seq analysis.
- (C) The plots visualize the UMAP embedding of Club-tracer (tdT⁺ZsG⁺) cells colored by each cluster.
- (D) Pseudotime trajectory plot reveals differentiation trajectories from progenitor cells toward alveolar epithelial cells.
- (E) The bar graph shows the enriched GO pathways in differential expression genes between H2-K1⁺ club cells and transient cells from Club-tracer.
- (F) The bar graph shows the enriched GO pathways in differential expression genes between transient cells and AT2 cells from Club-tracer.
- (G) The dot plot shows the expression levels of representative marker genes across each cluster in Club-tracer.
- (H) The plots visualize the UMAP embedding of BASC-tracer (tdT⁺ZsG⁺) cells colored by each cluster.
- (I) Pseudotime trajectory plot reveals differentiation trajectories from progenitor cells (BASC-like cells) toward alveolar epithelial cells.
- (J) The bar graph shows the enriched GO pathways in differential expression genes between transient cells and *Chil1*^{high} AT2 cells from BASC-tracer.
- (K) The dot plot shows the expression levels of representative marker genes across each cluster in BASC-tracer.
- (L) The heatmap shows the Pearson's correlation between AT2 subpopulations across the Club-, BASC-, and AT2-tracers.



(legend on next page)

injury (Figures 7I and 7J). We also found that the percentage of tdT⁺ cells expressing the ciliated cell marker Ace-Tub was significantly greater when Notch was deleted (Figure S7L), consistent with previous reports.^{37,38} These results suggested that the Notch signaling pathway plays distinct roles in regulating the conversion of club cells and BASCs into AT2 cells.

Given that inhibition of the Notch signaling in BASCs enhanced their differentiation into AT2 cells during lung regeneration, we next investigated whether constitutive activation of Notch signaling in BASCs blocks their cell fate transition. To specifically activate Notch in BASCs, we generated a new dual recombination reporter system *R26-RL-NICD-GFP* (Figure S7M). Only after Dre-rox and Cre-loxP recombinations, the two Stops were excised, and the constitutively active Notch intracellular domain (NICD) and GFP would be co-expressed in Dre⁺Cre⁺ cells. We generated *Scgb1a1-CreER;Sftpc-DreER;R26-RL-NICD-GFP* mice to induce Notch signaling activation specifically in BASCs and genetically labeled them with GFP (BASC-tracer3; Figures 7K–7M and S7N). *Scgb1a1-CreER;Sftpc-DreER;R26-RL-GFP* mice were used as the control group (Figure 7K). We then induced bleomycin injury to test the effect of Notch activation on BASCs differentiation after injury (Figure 7K). Immunostaining data showed that BASCs participated in alveolar regeneration by contributing to AT2 cells in control mice after injury (Figure 7N), which was consistent with our previous findings.^{12,14,32} However, we found that GFP-labeled cells were massively expanded and clogged the BADJ in the NICD-overexpressing mice post-injury (Figure 7N). Immunostaining showed that these Notch-activated cells were rarely Sftpc⁺ AT2 cells or T1a⁺ AT1 cells but were Scgb1a1⁺ and E-cad⁺ epithelial cells (Figures 7N and 7O). Taken together, these results indicate that the Notch signaling pathway plays distinct roles in club-cell- and BASC-mediated regeneration of AT2 cells during lung repair and regeneration (Figure 7P).

DISCUSSION

Recent studies have suggested that Hopx⁺ AT1 and Scgb1a1⁺ club cells serve as important sources of AT2 cells after alveolar injury. However, the genetic tools used in these studies were not specific. Here, we first showed that the *Hopx-CreER* tool labeled not only AT1 cells but also club cells, BASCs, ciliated cells, and AT2 cells in the lung. Similarly, the *Scgb1a1-CreER*

tool targeted not only club cells but also BASCs and a subset of AT2 cells. This non-specific labeling interferes with the lineage tracing results of AT1 and club cells, leading to controversial conclusions. In this study, we utilized Cre-loxP- and Dre-rox-mediated dual recombination systems to achieve specific labeling of these lung epithelial cells and then systematically elucidated the cellular origin of AT2 cells after lung injury. Our lineage tracing data suggest that AT1 cells do not contribute to AT2 cells during lung homeostasis, injury, and repair. For club cells, BASCs, and AT2 cells, we achieved simultaneous and specific labeling of these three cell populations with distinct genetic reporters in the same individual mouse. These systematic applications of dual recombinase-mediated intersectional genetic strategies enable precise labeling and tracing of diverse lung epithelial cell populations.

In this study, we used dual recombinase-mediated genetic strategy to compare the roles of club cells and BASCs in alveolar injuries, and we used scRNA-seq and cell-specific gene manipulation to explore the underlying molecular regulation of cell-fate transitions. By using different alveolar injury models, we revealed that their cellular plasticity was positively correlated with the degree of alveolar damage. In the PNx-induced injury model, the regeneration of AT2 cells primarily relies on self-renewal, with minimal contribution from club cells and BASCs. In the bleomycin-induced injury model, club cells and BASCs regenerate a large proportion of AT2 and AT1 cells. While the conversion efficiency of the individual club to AT2 cells was lower than that of BASCs, club cells significantly outnumbered BASCs in the lung and therefore generated more AT2 cells than BASCs in the injured lung. Additionally, there is a difference in the speed and fidelity of alveolar repair from club cells and BASCs. To further investigate the potential of club cells, we developed two extensive alveolar injury models, and the club cells exhibited remarkable cell plasticity and could regenerate most of the damaged alveoli. The large expansion of club-derived AT2 cells may be due to the depletion of AT2 progenitor cells. It is possible that the decreasing number of p21⁺ AT2 cells could be due to their death or differentiation into AT1 cells. Additionally, club-derived AT2 cells may have a greater survival advantage over their neighboring p21⁺ AT2 cells during chronic repair through cell competition.

In summary, our study provides more precise genetic lineage tracing evidence to improve our understanding of pulmonary cell

Figure 7. Notch signaling distinctly regulates the conversion of club cells and BASCs into AT2 cells

- (A) A violin plot showing the Notch signaling enrichment score across the indicated cell clusters in the Club-tracer.
(B) A plot showing the expression of Hes1 along the differentiation trajectories from H2-K1⁺ club cells toward AT2 cells.
(C) A violin plot showing the Notch signaling enrichment score across the indicated cell clusters in the BASC-tracer.
(D) A plot showing the expression of Hes1 along the differentiation trajectories from BASC-like cells toward Chil1^{high} AT2 cells.
(E and F) A schematic diagram illustrating the experimental design.
(G) Immunostaining of tdT, ZsG, and Sftpc on lung sections.
(H) Quantification of the percentage of lineage labeled Sftpc⁺ AT2 cells after bleomycin injury in (G). *****p* < 0.0001; ***p* = 0.0009; *p* = 0.0140.
(I and J) Flow cytometric analysis (I) and quantification (J) of the percentage of EpCAM⁺Lysotraker⁺CD45⁻ AT2 cells that express tdT or ZsG. ****p* = 0.0004; **p* = 0.0313; *p* = 0.6874; ns, non-significant.
(K) A schematic diagram illustrating the experimental design.
(L, M) A schematic diagram illustrating the experimental strategy.
(N) Immunostaining of GFP and Sftpc on lung sections of control and mutant mice.
(O) Immunostaining of GFP, Scgb1a1, T1a, and E-cadherin (E-cad) on lung sections.
(P) A cartoon image showing that Notch signaling regulates conversion of club cells and BASCs to AT2 cells.
Data are mean ± SD; *n* = 4–6. Yellow bars, 1 mm; white bars, 100 μm.

plasticity. The intersectional genetic lineage tracing results reveal the origins of and the mechanism for renewing AT2 cells during alveolar repair, which provides new insights for lung regeneration and potentially for disease therapy. The new strategies reported here could be widely used for studying diverse cell origins and cell fates in tissue development, regeneration, and diseases in many other contexts.³⁹

Limitations of the study

In this study, we investigated the AT1 plasticity during PNX-, bleomycin-, or hyperoxia-induced lung injury, which is a non-exhaustive list of the potential types of injury or the cell types that could be involved. Therefore, it cannot be ruled out that AT1 cells may have the potential to generate AT2 cells in other types of lung-injury models. Additionally, single-cell analysis in this study uncovered multiple intermediate clusters within the conversions of club-cells-to-AT2-cells and BASCs-to-AT2-cells after bleomycin-induced injury. A definitive demonstration of the cell fate and function of intermediate cells *in vivo* requires the future generation of a series of new genetic tools to target these specific cell clusters with the markers identified by scRNA-seq.

STAR★METHODS

Detailed methods are provided in the online version of this paper and include the following:

- **KEY RESOURCES TABLE**
- **RESOURCE AVAILABILITY**
 - Lead contact
 - Materials availability
 - Data and code availability
- **EXPERIMENTAL MODEL AND STUDY PARTICIPANT DETAILS**
 - Mice
- **METHOD DETAILS**
 - Pneumonectomy
 - Bleomycin-induced alveolar injury
 - Hyperoxia-induced lung injury
 - Genomic PCR
 - Tissue collection and immunofluorescent staining
 - Lung-tissue dissociation and flow cytometry
 - ROS measurement by flow cytometry
 - Single-cell RNA sequencing
- **QUANTIFICATION AND STATISTICAL ANALYSIS**

ACKNOWLEDGMENTS

This study was supported by the National Natural Science Foundation of China (82088101, 32370897, 32100648); CAS Project for Young Scientists in Basic Research (YSBR-012); National Key Research and Development Program of China (2019YFA0802000, 2019YFA0110403, 2020YFA0803202, 2023YFA1800700, 2023YFA1801300); Shanghai Pilot Program for Basic Research-CAS, Shanghai Branch (JCYJ-SHFY-2021-0); Research Funds of Hangzhou Institute for Advanced Study (2022ZZ01015, B04006C01600515); Shanghai Municipal Science and Technology Major Project; and the New Cornerstone Science Foundation through the New Cornerstone Investigator Program and the XPLOER PRIZE. We thank Kathy O. Lui for editing the manuscript, Hongkui Zeng for sharing the *R26-tdT* and *R26-RSR-LSL-tdT* mice, and Hongbin Ji for sharing the *Sftpc-DreER* mice. We thank Shanghai Model Organisms Cen-

ter for mouse generation and Jinmei Zhang, Baojin Wu, Guoyuan Chen, and Xiaorui Zhang for animal husbandry. We also thank the members of the cell platform in CEMCS and Yanqing Qin of SINH for assistance in flow cytometry and microscope.

AUTHOR CONTRIBUTIONS

K.L. and B.Z. designed the study, analyzed the data, and wrote the manuscript; K.L., X.M., M.T., Z. Lv, X. Huang, H.J., X. Han, X.L., W.P., and H.Z. bred the mice and performed experiments; Z. Liu performed and analyzed the scRNA-seq experiments; B.Z. conceived, supervised, and organized the study.

DECLARATION OF INTERESTS

The authors declare no competing interests.

Received: September 15, 2023

Revised: January 7, 2024

Accepted: March 8, 2024

Published: April 4, 2024

REFERENCES

1. Basil, M.C., Katzen, J., Engler, A.E., Guo, M., Herriges, M.J., Kathiriya, J.J., Windmueller, R., Ysasi, A.B., Zacharias, W.J., Chapman, H.A., et al. (2020). The Cellular and Physiological Basis for Lung Repair and Regeneration: Past, Present, and Future. *Cell Stem Cell* 26, 482–502. <https://doi.org/10.1016/j.stem.2020.03.009>.
2. Hogan, B.L.M., Barkauskas, C.E., Chapman, H.A., Epstein, J.A., Jain, R., Hsia, C.C.W., Niklason, L., Calle, E., Le, A., Randell, S.H., et al. (2014). Repair and regeneration of the respiratory system: complexity, plasticity, and mechanisms of lung stem cell function. *Cell Stem Cell* 15, 123–138. <https://doi.org/10.1016/j.stem.2014.07.012>.
3. Rawlins, E.L., Okubo, T., Xue, Y., Brass, D.M., Auten, R.L., Hasegawa, H., Wang, F., and Hogan, B.L.M. (2009). The role of Scgb1a1+ Clara cells in the long-term maintenance and repair of lung airway, but not alveolar, epithelium. *Cell Stem Cell* 4, 525–534. <https://doi.org/10.1016/j.stem.2009.04.002>.
4. Ouadah, Y., Rojas, E.R., Riordan, D.P., Capostagno, S., Kuo, C.S., and Krasnow, M.A. (2019). Rare Pulmonary Neuroendocrine Cells Are Stem Cells Regulated by Rb, p53, and Notch. *Cell* 179, 403–416.e23. <https://doi.org/10.1016/j.cell.2019.09.010>.
5. Song, H., Yao, E., Lin, C., Gacayan, R., Chen, M.H., and Chuang, P.T. (2012). Functional characterization of pulmonary neuroendocrine cells in lung development, injury, and tumorigenesis. *Proc. Natl. Acad. Sci. USA* 109, 17531–17536. <https://doi.org/10.1073/pnas.1207238109>.
6. Barkauskas, C.E., Cronic, M.J., Rackley, C.R., Bowie, E.J., Keene, D.R., Stripp, B.R., Randell, S.H., Noble, P.W., and Hogan, B.L.M. (2013). Type 2 alveolar cells are stem cells in adult lung. *J. Clin. Invest.* 123, 3025–3036. <https://doi.org/10.1172/JCI68782>.
7. Wang, Y., Tang, Z., Huang, H., Li, J., Wang, Z., Yu, Y., Zhang, C., Li, J., Dai, H., Wang, F., et al. (2018). Pulmonary alveolar type I cell population consists of two distinct subtypes that differ in cell fate. *Proc. Natl. Acad. Sci. USA* 115, 2407–2412. <https://doi.org/10.1073/pnas.1719474115>.
8. Nabhan, A.N., Brownfield, D.G., Harbury, P.B., Krasnow, M.A., and Desai, T.J. (2018). Single-cell Wnt signaling niches maintain stemness of alveolar type 2 cells. *Science* 359, 1118–1123. <https://doi.org/10.1126/science.aam6603>.
9. Zacharias, W.J., Frank, D.B., Zepp, J.A., Morley, M.P., Alkhaleel, F.A., Kong, J., Zhou, S., Cantu, E., and Morrissey, E.E. (2018). Regeneration of the lung alveolus by an evolutionarily conserved epithelial progenitor. *Nature* 555, 251–255. <https://doi.org/10.1038/nature25786>.
10. Wang, Z., Wei, D., Bin, E., Li, J., Jiang, K., Lv, T., Mao, X., Wang, F., Dai, H., and Tang, N. (2023). Enhanced glycolysis-mediated energy production in

- alveolar stem cells is required for alveolar regeneration. *Cell Stem Cell* 30, 1028–1042.e7. <https://doi.org/10.1016/j.stem.2023.07.007>.
- Kim, C.F.B., Jackson, E.L., Woolfenden, A.E., Lawrence, S., Babar, I., Vogel, S., Crowley, D., Bronson, R.T., and Jacks, T. (2005). Identification of bronchioalveolar stem cells in normal lung and lung cancer. *Cell* 121, 823–835. <https://doi.org/10.1016/j.cell.2005.03.032>.
 - Liu, Q., Liu, K., Cui, G., Huang, X., Yao, S., Guo, W., Qin, Z., Li, Y., Yang, R., Pu, W., et al. (2019). Lung regeneration by multipotent stem cells residing at the bronchioalveolar-duct junction. *Nat. Genet.* 51, 728–738. <https://doi.org/10.1038/s41588-019-0346-6>.
 - Salwig, I., Spitznagel, B., Vazquez-Armendariz, A.I., Khalooghi, K., Guenther, S., Herold, S., Szibor, M., and Braun, T. (2019). Bronchioalveolar stem cells are a main source for regeneration of distal lung epithelia in vivo. *EMBO J.* 38, e102099. <https://doi.org/10.15252/embj.2019102099>.
 - Liu, K., Tang, M., Liu, Q., Han, X., Jin, H., Zhu, H., Li, Y., He, L., Ji, H., and Zhou, B. (2020). Bi-directional differentiation of single bronchioalveolar stem cells during lung repair. *Cell Discov.* 6, 1. <https://doi.org/10.1038/s41421-019-0132-8>.
 - Jain, R., Barkauskas, C.E., Takeda, N., Bowie, E.J., Aghajanian, H., Wang, Q., Padmanabhan, A., Manderfield, L.J., Gupta, M., Li, D., et al. (2015). Plasticity of Hopx(+) type I alveolar cells to regenerate type II cells in the lung. *Nat. Commun.* 6, 6727. <https://doi.org/10.1038/ncomms7727>.
 - Penkala, I.J., Liberti, D.C., Pankin, J., Sivakumar, A., Kremp, M.M., Jayachandran, S., Katzen, J., Leach, J.P., Windmueller, R., Stolz, K., et al. (2021). Age-dependent alveolar epithelial plasticity orchestrates lung homeostasis and regeneration. *Cell Stem Cell* 28, 1775–1789.e5. <https://doi.org/10.1016/j.stem.2021.04.026>.
 - Liberti, D.C., Liberti Iii, W.A., Kremp, M.M., Penkala, I.J., Cardenas-Diaz, F.L., Morley, M.P., Babu, A., Zhou, S., Fernandez Iii, R.J., and Morrisey, E.E. (2022). Klf5 defines alveolar epithelial type 1 cell lineage commitment during lung development and regeneration. *Dev. Cell* 57, 1742–1757.e5. <https://doi.org/10.1016/j.devcel.2022.06.007>.
 - Shiraishi, K., Shah, P.P., Morley, M.P., Loebel, C., Santini, G.T., Katzen, J., Basil, M.C., Lin, S.M., Planer, J.D., Cantu, E., et al. (2023). Biophysical forces mediated by respiration maintain lung alveolar epithelial cell fate. *Cell* 186, 1478–1492.e15. <https://doi.org/10.1016/j.cell.2023.02.010>.
 - Kathiriya, J.J., Brumwell, A.N., Jackson, J.R., Tang, X., and Chapman, H.A. (2020). Distinct Airway Epithelial Stem Cells Hide among Club Cells but Mobilize to Promote Alveolar Regeneration. *Cell Stem Cell* 26, 346–358.e4. <https://doi.org/10.1016/j.stem.2019.12.014>.
 - Choi, J., Jang, Y.J., Dabrowska, C., Ilich, E., Evans, K.V., Hall, H., Janes, S.M., Simons, B.D., Koo, B.K., Kim, J., and Lee, J.H. (2021). Release of Notch activity coordinated by IL-1beta signalling confers differentiation plasticity of airway progenitors via Fosl2 during alveolar regeneration. *Nat. Cell Biol.* 23, 953–966. <https://doi.org/10.1038/s41556-021-00742-6>.
 - Strunz, M., Simon, L.M., Ansari, M., Kathiriya, J.J., Angelidis, I., Mayr, C.H., Tsidiridis, G., Lange, M., Mattner, L.F., Yee, M., et al. (2020). Alveolar regeneration through a Krt8+ transitional stem cell state that persists in human lung fibrosis. *Nat. Commun.* 11, 3559. <https://doi.org/10.1038/s41467-020-17358-3>.
 - Juul, N.H., Yoon, J.K., Martinez, M.C., Rishi, N., Kazadaeva, Y.I., Morri, M., Neff, N.F., Trope, W.L., Shrager, J.B., Sinha, R., and Desai, T.J. (2023). KRAS(G12D) drives lepidic adenocarcinoma through stem-cell reprogramming. *Nature* 619, 860–867. <https://doi.org/10.1038/s41586-023-06324-w>.
 - Desai, T.J., Brownfield, D.G., and Krasnow, M.A. (2014). Alveolar progenitor and stem cells in lung development, renewal and cancer. *Nature* 507, 190–194. <https://doi.org/10.1038/nature12930>.
 - Frank, D.B., Penkala, I.J., Zepp, J.A., Sivakumar, A., Linares-Saldana, R., Zacharias, W.J., Stolz, K.G., Pankin, J., Lu, M., Wang, Q., et al. (2019). Early lineage specification defines alveolar epithelial ontogeny in the murine lung. *Proc. Natl. Acad. Sci. USA* 116, 4362–4371. <https://doi.org/10.1073/pnas.1813952116>.
 - Guo, M., Du, Y., Gokey, J.J., Ray, S., Bell, S.M., Adam, M., Sudha, P., Perl, A.K., Deshmukh, H., Potter, S.S., et al. (2019). Single cell RNA analysis identifies cellular heterogeneity and adaptive responses of the lung at birth. *Nat. Commun.* 10, 37. <https://doi.org/10.1038/s41467-018-07770-1>.
 - Madisen, L., Zwingman, T.A., Sunkin, S.M., Oh, S.W., Zariwala, H.A., Gu, H., Ng, L.L., Palmiter, R.D., Hawrylycz, M.J., Jones, A.R., et al. (2010). A robust and high-throughput Cre reporting and characterization system for the whole mouse brain. *Nat. Neurosci.* 13, 133–140. <https://doi.org/10.1038/nn.2467>.
 - Han, X., Zhang, Z., He, L., Zhu, H., Li, Y., Pu, W., Han, M., Zhao, H., Liu, K., Li, Y., et al. (2021). A suite of new Dre recombinase drivers markedly expands the ability to perform intersectional genetic targeting. *Cell Stem Cell* 28, 1160–1176.e7. <https://doi.org/10.1016/j.stem.2021.01.007>.
 - He, L., Li, Y., Li, Y., Pu, W., Huang, X., Tian, X., Wang, Y., Zhang, H., Liu, Q., Zhang, L., et al. (2017). Enhancing the precision of genetic lineage tracing using dual recombinases. *Nat. Med.* 23, 1488–1498. <https://doi.org/10.1038/nm.4437>.
 - Zhang, H., Pu, W., Li, G., Huang, X., He, L., Tian, X., Liu, Q., Zhang, L., Wu, S.M., Sucov, H.M., and Zhou, B. (2016). Endocardium Minimally Contributes to Coronary Endothelium in the Embryonic Ventricular Free Walls. *Circ. Res.* 118, 1880–1893. <https://doi.org/10.1161/CIRCRESAHA.116.308749>.
 - Chung, M.I., and Hogan, B.L.M. (2018). Ager-CreER(T2): A New Genetic Tool for Studying Lung Alveolar Development, Homeostasis, and Repair. *Am. J. Respir. Cell Mol. Biol.* 59, 706–712. <https://doi.org/10.1165/rcmb.2018-0125OC>.
 - Madisen, L., Garner, A.R., Shimaoka, D., Chuong, A.S., Klapoetke, N.C., Li, L., van der Bourg, A., Niino, Y., Ego, L., Monetti, C., et al. (2015). Transgenic Mice for Intersectional Targeting of Neural Sensors and Effectors with High Specificity and Performance. *Neuron* 85, 942–958. <https://doi.org/10.1016/j.neuron.2015.02.022>.
 - Liu, K., Tang, M., Jin, H., Liu, Q., He, L., Zhu, H., Liu, X., Han, X., Li, Y., Zhang, L., et al. (2020). Triple-cell lineage tracing by a dual reporter on a single allele. *J. Biol. Chem.* 295, 690–700. <https://doi.org/10.1074/jbc.RA119.011349>.
 - Carlson, M.E., Hsu, M., and Conboy, I.M. (2008). Imbalance between pSmad3 and Notch induces CDK inhibitors in old muscle stem cells. *Nature* 454, 528–532. <https://doi.org/10.1038/nature07034>.
 - Pu, W., Han, X., He, L., Li, Y., Huang, X., Zhang, M., Lv, Z., Yu, W., Wang, Q.D., Cai, D., et al. (2020). A genetic system for tissue-specific inhibition of cell proliferation. *Development* 147, dev183830. <https://doi.org/10.1242/dev.183830>.
 - Kobayashi, Y., Tata, A., Konkimalla, A., Katsura, H., Lee, R.F., Ou, J., Banovich, N.E., Kropinski, J.A., and Tata, P.R. (2020). Persistence of a regeneration-associated, transitional alveolar epithelial cell state in pulmonary fibrosis. *Nat. Cell Biol.* 22, 934–946. <https://doi.org/10.1038/s41556-020-0542-8>.
 - Tian, X., He, L., Liu, K., Pu, W., Zhao, H., Li, Y., Liu, X., Tang, M., Sun, R., Fei, J., et al. (2020). Generation of a self-cleaved inducible Cre recombinase for efficient temporal genetic manipulation. *EMBO J.* 39, e102675. <https://doi.org/10.15252/embj.2019102675>.
 - Tsao, P.N., Vasconcelos, M., Izvolsky, K.I., Qian, J., Lu, J., and Cardoso, W.V. (2009). Notch signaling controls the balance of ciliated and secretory cell fates in developing airways. *Development* 136, 2297–2307. <https://doi.org/10.1242/dev.034884>.
 - Lafkas, D., Shelton, A., Chiu, C., de Leon Boenig, G., Chen, Y., Stawicki, S.S., Siltanen, C., Reichelt, M., Zhou, M., Wu, X., et al. (2015). Therapeutic antibodies reveal Notch control of transdifferentiation in the adult lung. *Nature* 528, 127–131. <https://doi.org/10.1038/nature15715>.
 - Liu, K., Jin, H., and Zhou, B. (2020). Genetic lineage tracing with multiple DNA recombinases: A user's guide for conducting more precise cell fate mapping studies. *J. Biol. Chem.* 295, 6413–6424. <https://doi.org/10.1074/jbc.REV120.011631>.

40. Han, M., Liu, Z., Liu, L., Huang, X., Wang, H., Pu, W., Wang, E., Liu, X., Li, Y., He, L., et al. (2023). Dual genetic tracing reveals a unique fibroblast subpopulation modulating cardiac fibrosis. *Nat. Genet.* *55*, 665–678. <https://doi.org/10.1038/s41588-023-01337-7>.
41. Sherman, B.T., Hao, M., Qiu, J., Jiao, X., Baseler, M.W., Lane, H.C., Imamichi, T., and Chang, W. (2022). DAVID: a web server for functional enrichment analysis and functional annotation of gene lists (2021 update). *Nucleic Acids Res.* *50*, W216–W221. <https://doi.org/10.1093/nar/gkac194>.
42. Arnold, K., Sarkar, A., Yram, M.A., Polo, J.M., Bronson, R., Sengupta, S., Seandel, M., Geijsen, N., and Hochedlinger, K. (2011). Sox2(+) adult stem and progenitor cells are important for tissue regeneration and survival of mice. *Cell Stem Cell* *9*, 317–329. <https://doi.org/10.1016/j.stem.2011.09.001>.
43. Rock, J.R., Barkauskas, C.E., Cronic, M.J., Xue, Y., Harris, J.R., Liang, J., Noble, P.W., and Hogan, B.L.M. (2011). Multiple stromal populations contribute to pulmonary fibrosis without evidence for epithelial to mesenchymal transition. *Proc. Natl. Acad. Sci. USA* *108*, E1475–E1483. <https://doi.org/10.1073/pnas.1117988108>.

STAR★METHODS

KEY RESOURCES TABLE

REAGENT or RESOURCE	SOURCE	IDENTIFIER
Antibodies		
Goat anti-GFP	Abcam	Cat#ab6662; RRID: AB_305635
Rabbit anti-GFP	Invitrogen	Cat#A11122; RRID:AB_2307355
ZsGreen	Clontech	Cat#632474; RRID:AB_2491179
Rabbit anti-tdTomato	Rockland	Cat#600-401-379; RRID: AB_2209751
Goat anti-tdTomato	Rockland	Cat#200-101-379; RRID: AB_2744552
Rat anti-tdTomato	Proteintech	Cat#5f8(abin334653); RRID: AB_2336064
Rabbit anti-Scgb1a1	Abcam	Cat#ab213203; RRID:AB_2650558
Goat anti-Scgb1a1	Santa Cruz	Cat#SC-9772; RRID:AB_2238819
Goat anti-E-cadherin	R&D system	Cat#AF748; RRID:AB_355568
Syrian Hamster anti-T1a	DSHB	Cat# 8.1.1; RRID:AB_531893
Rat anti-AGER	R&D system	Cat# MAB1179; RRID:AB_2289349
Rabbit anti-Insulin	Abcam	Cat# ab63820; RRID:AB_1925116
Rabbit anti-Keratin 5	Biolegend	Cat# 905504; RRID:AB_2616956
Rabbit anti-CGRP	Sigma	Cat# C8198; RRID:AB_259091
Goat anti-Scgb3a2	R&D system	Cat# AF3545; RRID:AB_2183543
Mouse anti-Acetylated-tubulin	Sigma	Cat# T7451; RRID:AB_609894
Rabbit anti-Sftpc	Millipore	Cat# ab3786; RRID:AB_91588
Rat anti-Lamp3	Novus Biologicals	Cat# DDX0191P-100; RRID:AB_2827532
Rabbit anti-p21	Abcam	Cat# ab188224; RRID:AB_2734729
Rabbit anti-Ki67	Abcam	Cat# ab15580; RRID:AB_443209
Goat anti-Troponin I	Abcam	Cat#ab56357; RRID: AB_880622
Rabbit anti-Lpcat1	Invitrogen	Cat#PA5-96311; RRID: AB_2808113
Rabbit anti-Etv5	Abcam	Cat#ab102010; RRID: AB_10711030
Rabbit anti-Aquaporin 3	Invitrogen	Cat#PA578811; RRID: AB_2745927
Sheep anti-Gdf15	Invitrogen	Cat#PA5-47839; RRID: AB_2576258
Rabbit anti-Cldn18	Invitrogen	Cat#700178; RRID: AB_2532290
Rat anti-Krt8	DSHB	Cat#Troma-I; RRID: AB_531826
Rabbit anti-Igfbp7	ABclonal	Cat#A4615; RRID: AB_2863310
Rat anti-Krt19	DSHB	Cat#TROMA-III; RRID: AB_2133570
Rat anti-Lgals3	Invitrogen	Cat#14-5301-85; RRID: AB_837133
Rat anti-Fstl1	R&D system	Cat#MAB17381; RRID: AB_2263013
Rabbit anti-Ptges	Invitrogen	Cat#PA5-60916; RRID: AB_2646108
Rabbit anti-mt-Cytb	Invitrogen	Cat#PA5-100740; RRID: AB_2850243
Rabbit anti-Lars2	Proteintech	Cat#17097-1-AP; RRID: AB_2132807
Rabbit anti-Cldn4	Invitrogen	Cat#36-4800; RRID: AB_2533262
Rabbit anti-Cxcl15	Abcam	Cat#ab197016; RRID: AB_2722677
Rabbit anti-CD74	Abcam	Cat#ab245692; RRID: AB_2924345
Mouse anti-Ptgs1	Invitrogen	Cat#35-8100; RRID: AB_2533223
Rabbit anti-Ereg	Sango Biotech	Cat#D163829; RRID: AB_3076716
Rabbit anti-H2afz	Invitrogen	Cat#PA5-21923; RRID: AB_11152068
Mouse anti-Abca3	Abcam	Cat#ab24751; RRID: AB_448287
Rabbit anti-Akap5	Invitrogen	Cat#PA5-101095; RRID: AB_2850539

(Continued on next page)

Continued

REAGENT or RESOURCE	SOURCE	IDENTIFIER
Mouse anti-8-OHdG	Abcam	Cat#ab48508; RRID: AB_867461
Mouse anti-4-HNE	Abcam	Cat#ab48506; RRID: AB_867452
Alexa donkey anti-rabbit 488	Invitrogen	Cat#A21206; RRID: AB_2535792
Alexa donkey anti-rabbit 555	Invitrogen	Cat#A31572; RRID: AB_162543
Alexa donkey anti-rabbit 647	Invitrogen	Cat#A31573; RRID: AB_2536183
Alexa donkey a-mouse 488	Invitrogen	Cat#A21202; RRID: AB_141607
Alexa donkey a-mouse 647	Invitrogen	Cat#A31571; RRID: AB_162542
Donkey anti-rat 647	Abcam	Cat#ab150155; RRID: AB_2813835
Donkey anti-rat 488	Invitrogen	Cat#a21208; RRID: AB_2535794
Donkey anti-goat 488	Invitrogen	Cat#A11055; RRID: AB_2534102
Donkey anti-goat 555	Invitrogen	Cat#A21432; RRID: AB_2535853
Donkey anti-goat 647	Invitrogen	Cat#A21447; RRID: AB_141844
Impress goat anti-rat	Vector Laboratories	Cat#MP-7444; RRID: AB_2336530
HRP-donkey- <i>anti</i> -rat	Jackson ImmunoResearch Inc	Cat#712-035-153; RRID: AB_2340639
Impress horse anti-rabbit	Vector Laboratories	Cat#MP-7401; RRID: AB_2336529

Chemicals, peptides, and recombinant proteins

Tamoxifen	Sigma	Cat#T5648
Collagenase type I	Gibco	Cat#17100017
DNase I	Worthington	Cat#LS002139
Bleomycin	Sigma	Cat#B8416
Dispase	Corning	Cat#354235
Elastase	Worthington Biochemical	Cat#LS002279

Critical commercial assays

CellROX Deep Red	Thermo Fisher	Cat#C10422
Click-iT Plus TUNEL kit	Thermo Fisher	Cat#C10619
Click-iT Plus TUNEL kit	Thermo Fisher	Cat#C10619
Chromium Next GEM Single Cell 5' Kit v2	10X Genomics	Cat# 1000263

Deposited data

Single Cell RNA-sequencing	This paper	GEO: GSE252588
Single Cell RNA-sequencing	Liu et al. ¹²	GEO: GSE118891
Codes used in this study	This paper	https://doi.org/10.5281/zenodo.10464757

Experimental models: Organisms/strains

Mouse: <i>Hopx-CreER</i>	The Jackson Laboratory	JAX:017606
Mouse: <i>Ager-CreER</i>	The Jackson Laboratory	JAX: 032771
Mouse: <i>Hopx-2A-DreER</i>	Han et al. ²⁷	N/A
Mouse: <i>Sox2-CreER</i>	The Jackson Laboratory	JAX: 017593
Mouse: <i>Scgb1a1-CreER</i>	The Jackson Laboratory	JAX: 016225
Mouse: <i>Sftpc-CreER</i>	The Jackson Laboratory	JAX: 028054
Mouse: <i>Sftpc-DreER</i>	Liu et al. ¹²	N/A
Mouse: <i>Sftpc-mGFP-DTR</i>	This paper	N/A
Mouse: <i>R26-tdT</i>	Madisen et al. ²⁶	JAX: 007909
Mouse: <i>R26-RSR-tdT</i>	Zhang et al. ²⁹	N/A
Mouse: <i>R26-RSR-LSL-tdT</i>	Madisen et al. ³¹	N/A
Mouse: <i>R26-NR2</i>	He et al. ²⁸	N/A
Mouse: <i>R26-TLR</i>	Liu et al. ³²	N/A
Mouse: <i>R26-rox-p21-GFP</i>	Pu et al. ³⁴	N/A
Mouse: <i>R26-LZL-tdT</i>	Tian et al. ³⁶	N/A

(Continued on next page)

Continued

REAGENT or RESOURCE	SOURCE	IDENTIFIER
Mouse: <i>R26-RL-NICD-GFP</i>	This paper	N/A
Mouse: <i>R26-RL-GFP</i>	Han et al. ⁴⁰	N/A
Software and algorithms		
Prism 9.3.1	GraphPad Software, Inc.	N/A
FlowJo software	Tree Star, Ashland, Ore	N/A
PhotoLine 23.02	https://www.pl32.com/	N/A
ImageJ	NIH	https://imagej.nih.gov/ij/
Cellranger V6.1.1	10X Genomics	https://www.10xgenomics.com/cn/support/software/cell-ranger
R 4.1.2	R Project	https://www.r-project.org/
Seurat V4.1.2	Satija Lab	https://satijalab.org/seurat/
DAVID	Sherman et al. ⁴¹	https://david.ncifcrf.gov
DBSCAN V1.1-10	https://doi.org/10.18637/jss.v091.i01	https://github.com/mhahsler/dbscan
Monocle3 V1.2.9	Trapnell Lab	https://cole-trapnell-lab.github.io/monocle3/
ClusterProfiler V4.2.2	Yu Lab	https://guangchuangyu.github.io/software/clusterProfiler/
Pheatmap V1.0.12	CRAN	https://cran.r-project.org/web/packages/pheatmap/
Other		
Hyperoxia chamber	BioSpherix	ProOx 110

RESOURCE AVAILABILITY

Lead contact

Further information and requests for resources and reagents should be directed to and will be fulfilled by the lead contact, Bin Zhou (zhoubin@sibs.ac.cn).

Materials availability

All materials in this work are available and will be shared by the [lead contact](#) upon reasonable request.

Data and code availability

- Single-cell RNA-seq data generated in this study have been deposited at GEO and are publicly available as of the date of publication. Accession numbers are listed in the [key resources table](#). Microscopy data reported in this paper will be shared by the [lead contact](#) upon request.
- All original code has been deposited at Zenodo and is publicly available as of the date of publication. DOIs are listed in the [key resources table](#).
- Any additional information required to reanalyze the data reported in this paper is available from the [lead contact](#) upon request.

EXPERIMENTAL MODEL AND STUDY PARTICIPANT DETAILS

Mice

All mouse experiments were approved by the Institutional Animal Care and Use Committee (IACUC) of the Center for Excellence in Molecular Cell Science, Chinese Academy of Sciences. All animal experiments were strictly performed within the committee's guidelines. *Hopx-CreER*, *Ager-CreER*, *Hopx-2A-DreER*; *Sox2-CreER*, *Scgb1a1-CreER*, *Sftpc-DreER*, *Sftpc-CreER*, *R26-tdT*, *R26-RSR-tdT*, *R26-RSR-LSL-tdT*, *R26-NR2*, *R26-TLR*, *R26-rox-P21-GFP*, *R26-LZL-tdT*, and *R26-RL-GFP* mice lines were described previously.^{3,12,15,16,26–32,34,36,40,42,43} For the *R26-RL-NICD-GFP* mouse line, the *CAG-rox-stop-rox-loxP-stop-loxP-NICD-2A-GFP* sequence was inserted into the *Rosa26* locus as *R26-RL-NICD-GFP* by Shanghai Model Organisms Center, Inc. (SMOC). For the *Sftpc-mGFP-DTR* mouse line, the *membrane GFP (mGFP)-2A-diphtheria toxin receptor (DTR)* sequence was inserted into the 5' UTR of the endogenous *Sftpc* gene locus via homologous recombination. All adult experiments were performed on 7–20 weeks

old that were kept in a C57BL6/ICR mixed background. Both male and female mice were randomly used for experiments. All mice were fed the normal diet at the Specific Pathogen Free (SPF) animal laboratory of the Center for Excellence in Molecular Cell Science. The living environment of the animal laboratory was suitable, with 20°C–25°C temperature, 30–70% humidity, and a 12-h light-dark cycle. The mice were given 0.2 mg/g Tam (Sigma, T5648) by oral gavage. The strains of mice used for each experimental strategy are indicated in the figures. All new genetic mice were generated by Shanghai Model Organisms Center, Inc. (SMOC).

METHOD DETAILS

Pneumonectomy

Pneumonectomy (PNX) was performed on adult mice as previously reported.¹⁵ Mice were anesthetized with isoflurane and then placed on a heated pad. The limbs were fixed on the pad and the trachea was intubated with isoflurane. After disinfecting the chest, the internal chest was exposed by incising the fifth left intercostal rib. The hilum of the left lung was gently tied by using a 5-0 silk suture. Next, the left lung was resected and then the incision was closed and disinfected. The mice were kept warm on the pad until they were sober. The sham groups of mice performed the same surgical procedure except for the resection of the left lung. Then the lung tissues were collected after 3 weeks for analysis.

Bleomycin-induced alveolar injury

Bleomycin (Sigma B8416) was used to induce alveolar injury as previously reported.¹² Bleomycin was freshly dissolved in (phosphate-buffered saline) PBS at a concentration of 10 U/mL and stored at –80°C. The stock solution should be diluted to 1 U/mL with PBS before use. The adult mice were treated with 2 U/kg bleomycin or vehicle (PBS) by intratracheal instillation for alveolar injury. Then the lung tissues were collected at indicated time for analysis.

Hyperoxia-induced lung injury

Adult mice were given 200 mg/kg Tam as indicated doses by oral gavage and exposed to hyperoxia for 3 days at 95% oxygen after 3 weeks washout as previously reported.¹⁶ In brief, adult mice were housed in a chamber equipped with an oxygen controller (ProOx 110, BioSpherix) with medical grade 99.999% O₂ delivered continuously to maintain chamber O₂ levels at 95% to induce the alveolar epithelium injury. All mice in the chamber were provided with an additional nestlet and daily monitored to ensure habitable environment. After 3 days, mice were removed from hyperoxia and allowed to recover at room air for 7 days before harvesting the lungs.

Genomic PCR

Genomic DNA was prepared from the embryonic yolk sac or the transgenic mouse tails.

Tissues were lysed by incubation with lysis buffer (100 mM Tris HCl, pH 7.8, 5 mM EDTA, 0.2% SDS, 200 mM NaCl, and 100 μg/mL proteinase K) overnight at 55°C, and this was followed by centrifugation at maximum speed (21,130 × *g*) for 5 min to obtain supernatants with genomic DNA. DNA was precipitated with isopropanol, washed in 70% ethanol, and dissolved in deionized water. All embryos and mice were genotyped with genomic PCR as described previously.

Tissue collection and immunofluorescent staining

The immunofluorescent staining protocol was performed as previously reported.¹² Briefly, the mice were killed and the lungs were collected in 6-well plates, then fixed the lungs in 4% paraformaldehyde (PFA) for 1 h at 4°C. After washing with PBS in 3 times, the lungs were dehydrated in 30% sucrose (dissolved in 1 × PBS) overnight at 4°C. The lungs were embedded in OCT (Sakura). 10–12 μm frozen sections were collected on slides. For immunofluorescent staining, slides were dried at room temperature and then washed in PBS several times to remove OCT. Next, the slides were blocked in 5% PBSST buffer (0.1% Triton X-100 and 5% donkey serum in 1 × PBS) for 30 min at room temperature, then incubated with primary antibodies overnight at 4°C. Primary antibodies were used: Scgb1a1 (Santa Cruz, SC-9772, 1:200), Scgb1a1 (Abcam, ab213203, 1:300), tdTomato (Rockland, 600-401-379, 1:1000), tdTomato (Rockland, 200-101-379, 1:500), E-cadherin (R&D system, AF748, 1:500), T1a (DSHB, 8.1.1, 1:100), TNNI3 (Abcam, ab56357, 1:200), Insulin (Abcam, ab63820, 1:500), Keratin 5 (Biolegend, 905504, 1:500), CGRP (Sigma, C8198, 1:500), Scgb3a2 (R&D system, AF3545-SP, 1:500), Acetylated-tubulin (Sigma, T7451, 1:300), Sftpc (Millipore, AB3786, 1:200), GFP (Abcam, ab6662, 1:500), ZsGreen (Clontech, 632474, 1:1000), AGER (R&D system, MAB1179-100, 1:200), p21 (Abcam, ab188224, 1:500), Ki67 (Abcam, ab15580-100ug, 1:400), Lamp3 (Novus Biologicals, 1006F7.05, 1:200), Lpcat1 (Invitrogen, PA5-96311, 1:200), Etv5 (Abcam, ab102010, 1:200), Aqp3 (Invitrogen, PA578811, 1:200), Gdf15 (Invitrogen, PA5-47839, 1:200), Cldn18 (Invitrogen, 2535504, 1:200), Krt8 (DSHB, Troma-I-C, 1:200), Igfbp7 (ABclonal, A4615, 1:50), Krt19 (DSHB, TROMA-III, 1:500), Lgals3 (Invitrogen, 14-5301-85, 1:100), Fstl1 (R&D system, MAB17381, 1:50), Ptges (Invitrogen, PA5-60916, 1:200), mt-Cytb (Invitrogen, PA5-100740, 1:200), LARS2 (Proteintech, 17097-1-AP, 1:20), Cldn4 (Invitrogen, 36-4800, 1:100), Cxcl15 (Abcam, ab197016, 1:100), CD74 (Abcam, ab245692, 1:50), Ptgs1 (Invitrogen, 35-8100, 1:50), Ereg (Sango Biotech, D163829-0100, 1:100), H2afz (Invitrogen, PA5-21923, 1:100), Abca3 (Abcam, ab24751, 1:50), Akap5 (Invitrogen, PA5-101095, 1:500), 8-OHdG (Abcam, ab48508, 1:100), 4-HNE (Abcam, ab48506, 1:100) The next day, slides were washed with PBS in 3 times to remove primary antibodies and then incubated with secondary antibodies for 40 min at room temperature. Next, after washing with PBS 3 times, the slides were mounted with a mounting medium. The secondary antibodies were Alexa donkey anti-rabbit 555 (Invitrogen, A31572), Alexa donkey anti-rabbit 488

(Invitrogen, A21206), Alexa donkey anti-rabbit 647 (Invitrogen, A31573), Alexa donkey anti-goat 488 (Invitrogen, A11055), Alexa donkey anti-goat 555 (Invitrogen, A21432), Alexa donkey anti-goat 647 (Invitrogen, A21447), Alexa donkey anti-mouse 647 (Invitrogen, A31571; 1:1000), Alexa donkey anti-rat 647 (Invitrogen, A21247), Alexa donkey anti-rat 488 (Invitrogen, A21208), Alexa goat anti-hamster 488 (Invitrogen, A21110). TUNEL assays were performed using the Click-iT Plus TUNEL Assay kit from ThermoFisher Scientific (C10619) by the manufacturer's protocol after secondary antibodies incubation. Immunostaining images were obtained by Olympus FV1200 confocal system and Zeiss 880 confocal system. Images were analyzed by ImageJ (NIH) software.

Lung-tissue dissociation and flow cytometry

Lung tissues were digested as previously described.¹² After the mice were killed, the lungs were perfused using cold PBS through the right ventricle to wash out the blood cell and then the protease solution (collagenase type I (500U/mL; Gibco 17100-017), elastase(4U/mL; Worthington Biochemical Corporation LS002279), dispase (5 U/mL; BD Biosciences 354235) and DNase I (0.33 U/mL; Worthington Biochemical Corporation LS002139) in DMEM (Gibco, 11965092)) was injected into the lungs through the trachea to the lung. After that, the lungs were minced into small pieces and incubated in 4 mL protease solution for 30 min at a 37°C shaker with frequent agitation. Subsequently, the tissue pieces were dissociated by pipetting and centrifuged at 1000 x g for 5 min at 4°C. After washing with DMEM, the pellet was resuspended in 3 mL 0.1% Trypsin-EDTA (Gibco, 25200072) with DNase I and incubated for 20 min at a 37°C shaker with agitation and pipetting. Then the DMEM with 10% FBS was added to terminate the digestion and the cells were filtered sequentially through 100 μm strainers and centrifuged at 1000 x g for 5 min at 4°C. The cell pellet was resuspended in 1 mL of red blood cell (RBC) lysis buffer (2–5 mL, eBioscience, 00-4333-57) at room temperature for 5 min followed by PBS dilution and then centrifuged at 1000 x g for 5 min at 4°C. Afterward, the cell precipitate was resuspended in Fc block (eBioscience, 14-0161, 1:100) for 5 min to block nonspecific antigens for further staining. The following antibodies were used: CD45 APC-eFluor 780 (eBioscience, 47-0451-82,1:200), TER-119 APC-eFluor 780 (eBioscience, 47-5921-82, 1:200), CD326 PE-Cy7 (eBioscience, 25-5791,1:200). After staining for 30 min at 4°C, the cells were washed in PBS followed by centrifugation. Then the cells were resuspended in PBS supplemented with DAPI and DnaseI, which were used to distinguish dead cells from living cells and to avoid cell adhesion respectively.

LysoTracker was used to distinguish AT2 cells from lung epithelial cells as previously reported for its selective accumulation in lamellar bodies in AT2 cells. For LysoTracker staining, the cells were resuspended in DMEM with LysoTracker (Invitrogen, LysoTracker Deep Red, L12492) and incubated at 37°C for 10–15 min. After incubation, the cells were centrifuged at 1000 x g for 5 min at 4°C followed by washing in PBS to elute the remaining LysoTracker and then centrifuged to obtain the cell precipitate. Thereafter, the cell pellets were resuspended in PBS supplemented with DAPI and DnaseI. Thermo Attune NxT was used for flow cytometry analysis. Sony MA900 was used for cell sorting. FACS data were analyzed with FlowJo 10.4 (FlowJo LLC).

ROS measurement by flow cytometry

For ROS measurement, the isolated primary cells were resuspended in DMEM with 5μM CellROX Deep Red (Thermo Fisher, C10422) and incubated at 37°C for 30 min. After incubation, the cells were centrifuged at 1000 x g for 5 min at 4°C and then washed in PBS 2–3 times followed by centrifugation to obtain the cell precipitate. Thereafter, the cell pellets were resuspended in PBS supplemented with DAPI and DnaseI to perform the next FACS analysis.

Single-cell RNA sequencing

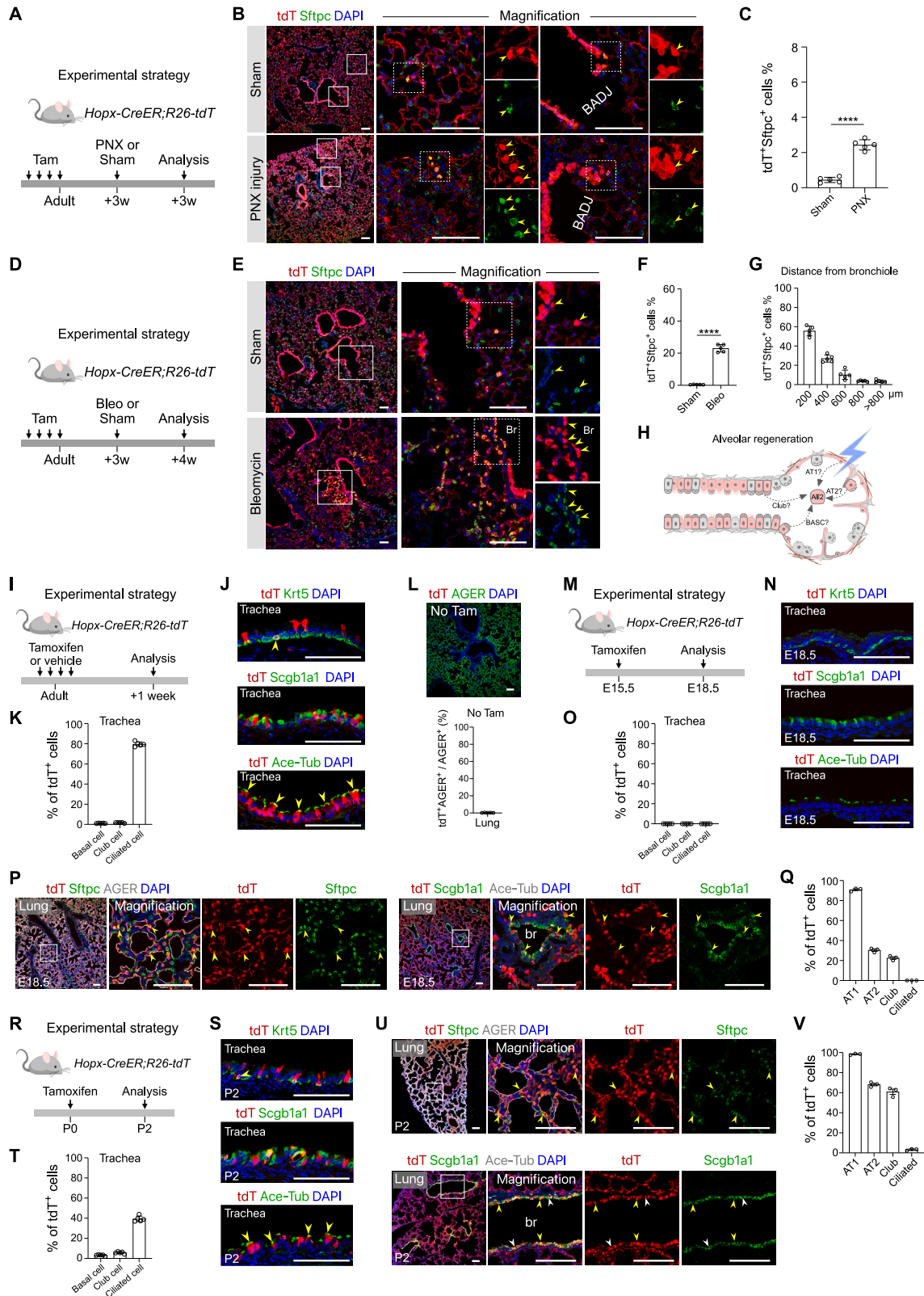
The cells isolated from bleomycin-treated mice were sorted using Fluorescence-Activated Cell Sorting (FACS) based on their cell lineage, relying specifically on fluorescent signals (AT2-tracer: ZsGreen⁺; BASC-tracer: ZsGreen⁺tdT⁺; Club-tracer: tdT⁺). For club cells to alveolar epithelium, lineage⁻ cells, ciliated cells, and an unknown cell type were excluded from analysis. For BASCs to alveolar epithelium, lineage⁻ cells, ciliated cells, and club cells were excluded from analysis. Cells with distinct lineages were loaded into the 10x Chromium controller to generate GEMs respectively, which were subsequently processed into single-cell 5' gene expression libraries using the Chromium Single Cell 5' Library Kit (v2 Chemistry). All samples were pooled for sequencing on the Illumina NovaSeq 6000 PE150 platform. Each single-cell RNA sequencing (scRNA-seq) dataset was processed using the Cell Ranger pipeline (v6.1.1) for alignment to the customized mouse reference genome (mm10), alignment filtering, barcode counting, and UMI counting. Quality control was initially performed using the R package Seurat (v4.1.2), excluding cells with fewer than 200 features and features expressed in fewer than 3 cells. Cells with a mitochondrial fraction above 0.1 (for AT2-tracer) or 0.08 (for Club-tracer and BASC-tracer), as well as fewer than 2500 genes (for BASC-tracer), 1300 genes (for AT2-tracer), or 1200 genes (for Club-tracer), and UMI counts less than 2000 were considered of low quality and consequently excluded from the analysis. The impact of cell cycle, the percentage of mitochondrial genes, and UMI counts were regressed out of each sample using the ScaleData(). For AT2-Tracer, only cells expressing ZsGreen with a value above zero will be included, while those showing any expression of tdT will be excluded. In the case of BASC-tracer, only cells with expression values above zero for both ZsGreen and tdT will be retained. In Club-tracer, only cells expressing tdT with a value greater than zero will be retained, while those demonstrating any expression of ZsGreen will be excluded. Furthermore, highly variable genes were used for principal-component analysis by RunPCA() and significant principal components were identified by ElbowPlot(). For AT2-tracer, 20 significant principal components were used as the input to RunUMAP() and clustering were performed by FindClusters() with parameter resolution = 0.3. In the case of BASC-tracer, 23 significant principal

components were used as the input to RunUMAP() and clustering were performed by FindClusters() with parameter resolution = 1. In Club-tracer, 14 significant principal components were used as the input to RunUMAP() and clustering were performed by FindClusters() with parameter resolution = 0.9. After dimension reduction and clustering by Seurat, DBSCAN R package (v1.1-10) was used to identify outlier cells with parameter eps = 0.6 for each tracer, which were subsequently removed from further analysis. For all integration analysis, top 40 dimensions were used as the input to FindIntegrationAnchors() and IntegrateData(). Differentially expressed genes were identified by FindAllMarkers() or FindMarkers() in Seurat package with customized parameters. Pseudotime trajectory was inferred by R package monocle3 (v1.2.9). The parameter use_partition = False was used in learn_graph() and default parameters were used in order_cells(). Hes1 expression along the inferred trajectory was visualized using plot_genes_in_pseudotime(). To identify the enriched signaling pathways and ontologies across the cell clusters, differentially expressed genes were analyzed using DAVID (<https://david.ncifcrf.gov>) through the Gene Ontology (GO) and Kyoto Encyclopedia of Genes and Genomes (KEGG) databases or ClusterProfiler (v4.2.2) with default parameters. Scaled data in Seurat objects were extracted and the mean values of the scaled score of the gene members in the Notch signaling pathway (GO: 0007219) were calculated and displayed as enrichment scores using VinPlot(). The Pearson's correlation of AT2 clusters across the three different tracers was calculated using cor() and a heatmap plot was generated using the R package pheatmap (v1.0.12). The raw and processed data from the single-cell RNA sequencing experiments have been deposited in the NCBI Gene Expression Omnibus database and can be accessed using the accession number GSE252588. The original code is also available on Zenodo via the following DOI link: <https://doi.org/10.5281/zenodo.10464757>.

QUANTIFICATION AND STATISTICAL ANALYSIS

All the mice were randomly assigned to groups. Mice were allocated randomly in experiments. Samples were processed arbitrarily. The researchers were blinded for image acquisition and quantification. The researchers were not blinded for mice treatment (Tam and injury) and sacrifice of control and experimental groups. Mice that died in the experiments were not used for analysis. At least 20 sections per sample and at least five 10× fields per section were analyzed in homeostasis and after injury in our study. For PNx, bleomycin, and hyperoxia injury (related to [Figures 2H, 2L, 2P, 3L, 4J, 5H, 5N, 5O, 7H, 7N, S1C, S1F, S1G, S4L, S4O, S4P, S5B, S5D–S5H, S5P, S5R, and S7K](#)), we analyzed the alveolar area of damaged regions. For [Figures 3H, 4G, and 5E](#), we analyzed the alveolar area of peribronchiolar regions. Statistical analyses were performed by using Prism software (GraphPad version 9.3.1). The normality of all samples was tested by using the Shapiro-Wilk test. All data were acquired in this study from at least three independent experiments and presented as mean values ±SD as indicated in figure legends. Two-tailed unpaired Student's *t* test was used for statistical analysis of the differences between the two groups (related to [Figures 2H, 2L, 2P, 3H, 3L, 4G, 4J, 5E, 5H, 5N, 7H, 7J, S1C, S1F, S4O, S4P, S5E–S5H, S6C, S7K, and S7L](#)). One-way ANOVA with Tukey's multiple comparisons test was used to compare the differences between multiple groups (related to [Figure 5O](#)). *****p* < 0.0001, ****p* < 0.001, ***p* < 0.01, and **p* < 0.05 was accepted as statistically significant. Specific quantification methods and *p* values are indicated in the figures and legends.

Supplemental figures



(legend on next page)

Figure S1. *Hopx-CreER*-based lineage tracing is not AT1 cell specific, related to Figure 1

- (A) A schematic diagram illustrating the experimental strategy.
- (B) Immunostaining for tdT and Sftpc on lung sections of *Hopx-CreER;R26-tdT* mice after PNX or sham treatment. Yellow arrowheads, tdT⁺Sftpc⁺ AT2 cells.
- (C) Quantification of the percentage of Sftpc⁺ cells expressing tdT in (B). Data are presented as mean ± SD; n = 5 mice per group. ****p < 0.0001. Statistical analysis was performed by two-tailed unpaired Student's *t* test.
- (D) A schematic diagram showing the experimental strategy.
- (E) Immunostaining for tdT and Sftpc on lung sections after bleomycin or sham treatment. Yellow arrowheads, tdT⁺Sftpc⁺ AT2 cells.
- (F) Quantification of the percentage of Sftpc⁺ cells expressing tdT in (E). Data are presented as mean ± SD; n = 5 mice per group. ****p < 0.0001. Statistical analysis was performed by two-tailed unpaired Student's *t* test.
- (G) Quantifying the percentage of tdT⁺Sftpc⁺ cells with different distances from the bronchioles. Data are presented as mean ± SD; n = 5 mice per group.
- (H) A cartoon image showing that the *Hopx-CreER* tool targets multiple types of pulmonary epithelial cells, which cannot distinguish the cellular origin of AT2 cells after alveolar injury.
- (I) A schematic diagram showing the experimental design.
- (J) Immunostaining for tdT, Krt5, Scgb1a1, and Ace-Tub on trachea sections of adult *Hopx-CreER;R26-tdT* after tamoxifen treatment. Yellow arrowheads, tdT⁺Krt5⁺ basal cells and tdT⁺Ace-Tub⁺ ciliated cells.
- (K) Quantification of the percentage of basal, club, and ciliated cells expressing tdT in (J). Data are presented as mean ± SD; n = 5 mice per group.
- (L) Immunostaining for tdT and AGER on lung sections of adult *Hopx-CreER;R26-tdT* mice without tamoxifen treatment (upper panel). Quantification of the percentage of AT1 cells was labeled by tdT (lower panel) without tamoxifen treatment. Data are presented as mean ± SD; n = 5 mice per group.
- (M) A schematic diagram showing the experimental design.
- (N) Immunostaining for tdT, Krt5, Scgb1a1, and Ace-Tub on E18.5 trachea sections of *Hopx-CreER;R26-tdT* mice after tamoxifen treatment.
- (O) Quantification of the percentage of basal, club, and ciliated cells of the trachea expressing tdT in (N). Data are presented as mean ± SD; n = 5 mice per group.
- (P) Immunostaining for tdT, Sftpc, AGER, Scgb1a1, and Ace-Tub on E18.5 lung sections of *Hopx-CreER;R26-tdT* embryos after tamoxifen treatment at E15.5. Yellow arrowheads, tdT⁺Sftpc⁺ AT2 cells or tdT⁺Scgb1a1⁺ club cells.
- (Q) Quantification of the percentage of AT1, AT2, club, and ciliated cells was labeled by tdT in (P). Data are presented as mean ± SD; n = 3 mice per group.
- (R) A schematic diagram illustrating the experimental design.
- (S) Immunostaining for tdT, Krt5, Scgb1a1, and Ace-Tub on P2 trachea sections of *Hopx-CreER;R26-tdT* mice after tamoxifen treatment at P0.
- (T) Quantification of the percentage of basal, club, and ciliated cells of the trachea was labeled by tdT in (S). Data are presented as mean ± SD; n = 5 mice per group.
- (U) Immunostaining for tdT, Sftpc, and AGER on postnatal 2 (P2) lung sections of *Hopx-CreER;R26-tdT* mice after tamoxifen treatment at P0 (upper panel). Yellow arrowheads, tdT⁺Sftpc⁺ AT2 cells. Immunostaining for tdT, Scgb1a1, and Ace-Tub on P2 lung sections of *Hopx-CreER;R26-tdT* mice after tamoxifen treatment at P0 (lower panel). Yellow arrowheads, tdT⁺Scgb1a1⁺ club cells. White arrowheads, tdT⁺Ace-Tub⁺ ciliated cells.
- (V) Quantification of the percentage of AT1, AT2, club, and ciliated cells expressing tdT in (U). Data are presented as mean ± SD; n = 3 mice per group. Data are presented as mean ± SD; n = 3–5 mice per group. Scale bars, 100 μm.

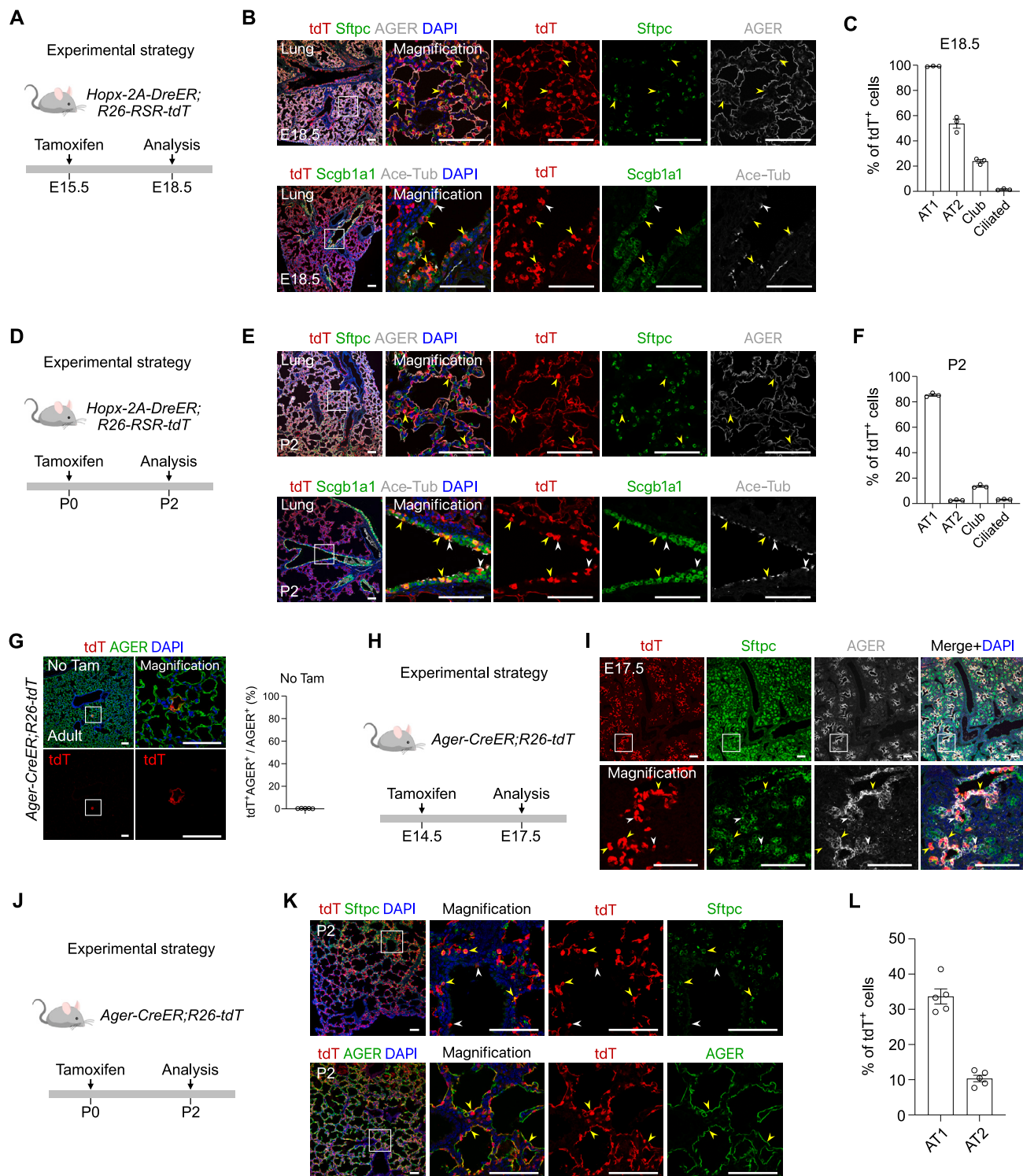


Figure S2. *Hox-2A-DreER*- and *Ager-CreER*-based lineage tracing is not AT1 cell specific, related to Figure 1

(A) A schematic diagram illustrating the experimental design.

(B) Immunostaining for tdT, Sftpc, AGER, Scgb1a1, and Ace-Tub on E18.5 lung sections of *Hox-2A-DreER; R26-RSR-tdT* embryos after tamoxifen treatment at E15.5. Yellow arrowheads, tdT⁺Sftpc⁺ AT2 cells or tdT⁺Scgb1a1⁺ club cells. White arrowheads, tdT⁺Ace-Tub⁺ ciliated cells.

(C) Quantification of the percentage of AT1, AT2, club, and ciliated cells expressing tdT in (B). Data are presented as mean ± SD; n = 3 mice per group.

(D) A schematic diagram illustrating the experimental design.

(legend continued on next page)

(E) Immunostaining for tdT, Sftpc, AGER, Scgb1a1, and Ace-Tub on P2 lung sections of *Hopx-2A-DreER;R26-RSR-tdT* embryos after tamoxifen treatment at P0. Yellow arrowheads, tdT⁺Sftpc⁺ AT2 cells or tdT⁺Scgb1a1⁺ club cells. White arrowheads, tdT⁺Ace-Tub⁺ ciliated cells.

(F) Quantification of the percentage of AT1, AT2, club, and ciliated cells was labeled by tdT in (E). Data are presented as mean \pm SD; n = 3 mice per group.

(G) Immunostaining for tdT and AGER on lung sections of adult *Ager-CreER;R26-tdT* mice without tamoxifen treatment (left panel). Quantification of the percentage of AT1 cells was labeled by tdT (right panel) without tamoxifen treatment. Data are presented as mean \pm SD; n = 5 mice per group.

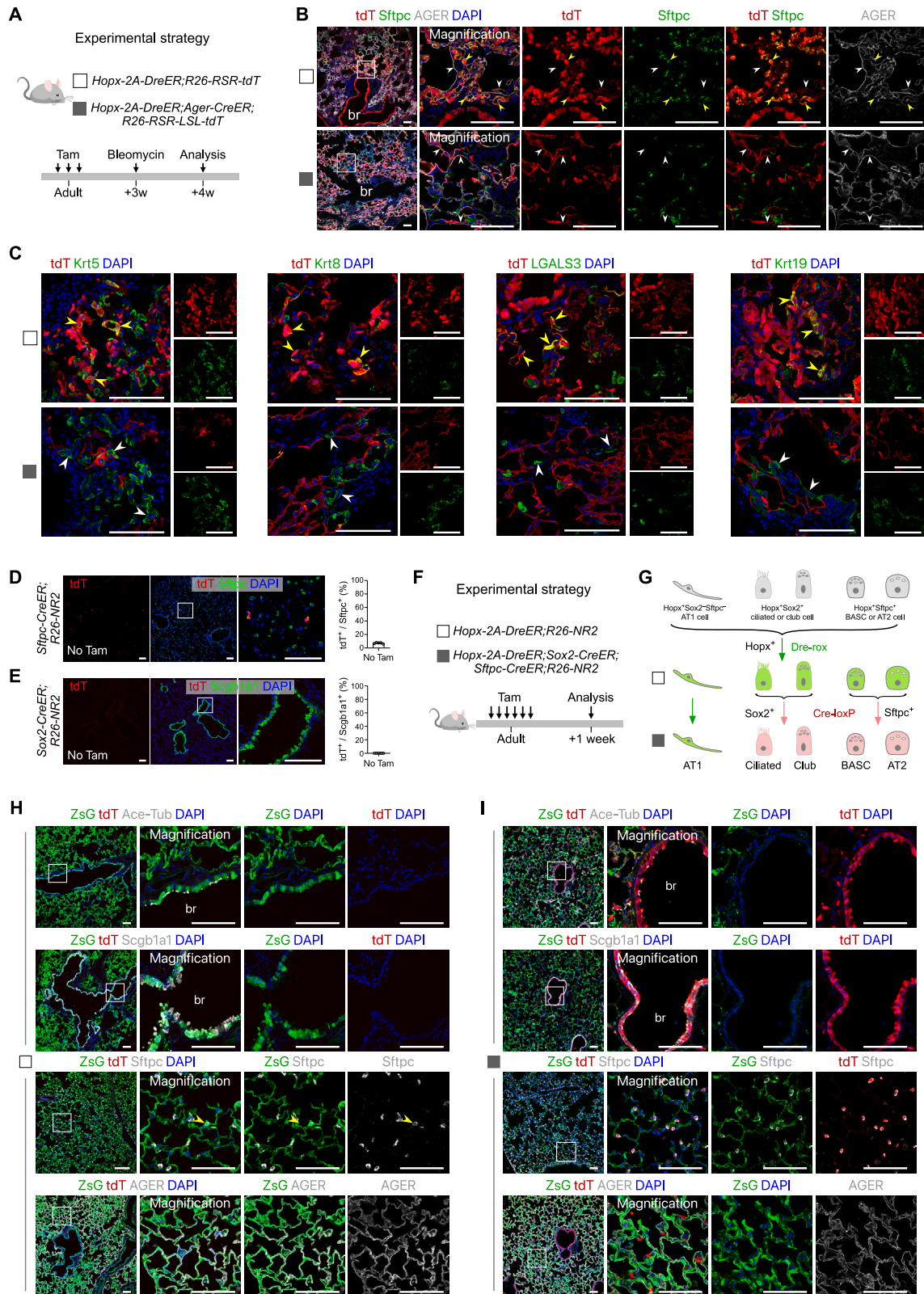
(H) A schematic diagram illustrating the experimental design.

(I) Immunostaining for tdT, Sftpc, and AGER on E17.5 lung sections of *Ager-CreER;R26-tdT* mice after tamoxifen treatment at E14.5. Yellow arrowheads, tdT⁺Sftpc⁺ cells. White arrowheads, tdT⁺ Sftpc⁺AGER⁺ cells.

(J) A schematic diagram illustrating the experimental design.

(K) Immunostaining for tdT, Sftpc, and AGER on P2 tissue sections of *Ager-CreER;R26-tdT* mice after tamoxifen treatment at P0. Yellow arrowheads, tdT⁺AGER⁺ AT1 cells or tdT⁺Sftpc⁺ AT2 cells.

(L) Quantification of the percentage of AT1 cells and AT2 cells expressing tdT in (K). Data are presented as mean \pm SD; n = 5 mice per group. Data are presented as mean \pm SD; n = 3–5 mice per group. Scale bars, 100 μ m.



(legend on next page)

Figure S3. AT1 cells do not contribute to AT2 cells after alveolar injury, related to Figures 2 and 3

(A) A schematic diagram illustrating the experimental design.

(B) Immunostaining for tdT, Sftpc, and AGER on lung sections of *Hopx-2A-DreER;R26-RSR-tdT* mice and *Hopx-2A-DreER;Ager-CreER;R26-RSR-LSL-tdT* mice after bleomycin injury. The *Hopx-2A-DreER;R26-RSR-tdT* mice were set as the positive control. Yellow arrowheads, tdT⁺Sftpc⁺ AT2 cells. White arrowheads, tdT⁺AGER⁺ AT1 cells.

(C) Immunostaining for tdT, Krt5, Krt8, LGALS3, and Krt19 on lung sections of *Hopx-2A-DreER;R26-RSR-tdT* mice and *Hopx-2A-DreER;Ager-CreER;R26-RSR-LSL-tdT* mice after bleomycin injury. Yellow arrowheads, tdT⁺Krt5⁺ cells, tdT⁺Krt8⁺ cells, tdT⁺LGALS3⁺ cells, or tdT⁺Krt19⁺ cells. White arrowheads, tdT⁻Krt5⁺ cells, tdT⁻Krt8⁺ cells, tdT⁻LGALS3⁺ cells, or tdT⁻Krt19⁺ cells.

(D) Immunostaining for tdT and Sftpc on lung sections of adult *Sftpc-CreER;R26-NR2* mice showed that small AT2 cells were labeled by tdT without tamoxifen treatment (left panel). Quantification of the percentage of Sftpc⁺ cells expressing tdT without tamoxifen treatment (right panel).

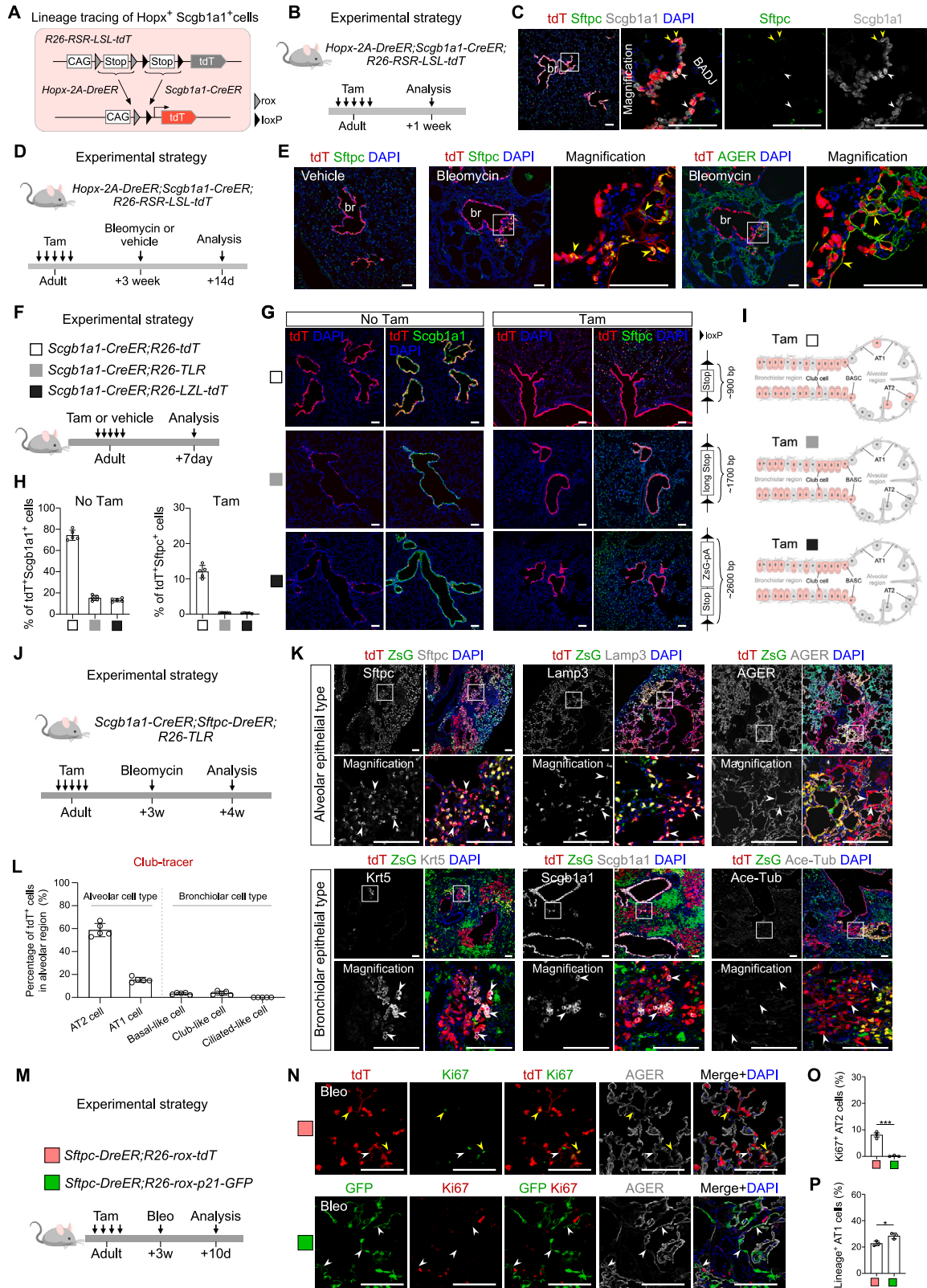
(E) Immunostaining for tdT and Sftpc on lung sections of adult *Sox2-CreER;R26-NR2* mice showed that no tdT signals were detected without tamoxifen treatment (left panel). Quantification of the percentage of bronchiolar cells expressing tdT without tamoxifen treatment (right panel).

(F) A schematic diagram illustrating the experimental design.

(G) A cartoon image showing that the Hopx⁺ AT1 cells were specifically labeled by ZsG, while the ciliated, club, BASCs, and AT2 cells were labeled by tdT in *Hopx-2A-DreER;Sox2-CreER;Sftpc-CreER;NR2* mice.

(H and I) Immunostaining for ZsG, tdT, Ace-Tub, Scgb1a1, Sftpc or AGER on lung sections of *Hopx-2A-DreER;R26-NR2* mice (H) and *Hopx-2A-DreER;Sox2-CreER;Sftpc-CreER;R26-NR2* mice (I) after tamoxifen treatment. Yellow arrowheads, ZsG⁺Sftpc⁺ AT2 cells.

Each immunostaining image is representative of 5 individual mice samples. Tam, tamoxifen. tdT, tdTomato. ZsG, ZsGreen. Bleo, bleomycin. Br, bronchiole. Data are presented as mean ± SD; n = 4–5 mice per group. Scale bars, 100 μm.



(legend on next page)

Figure S4. Contribution of club cells and BASCs to alveolar repair after lung injury, related to Figures 4 and 5

(A) A cartoon image showing the intersectional genetic strategy for lineage tracing of $Hopx^+Scgb1a1^+$ cells.

(B) A schematic diagram illustrating the experimental design.

(C) Immunostaining for tdT, Sftpc, and Scgb1a1 on lung sections of *Hopx-2A-DreER;Scgb1a1-CreER;R26-RSR-LSL-tdT* mice after tamoxifen treatment. White arrowheads, $tdT^+Sftpc^-Scgb1a1^+$ club cells; Yellow arrowheads, $tdT^+Sftpc^+Scgb1a1^+$ BASCs.

(D) A schematic diagram illustrating the experimental design.

(E) Immunostaining for tdT and Sftpc on lung sections of *Hopx-2A-DreER;Scgb1a1-CreER;R26-RSR-LSL-tdT* mice after vehicle (PBS) or bleomycin treatment. Yellow arrowheads, tdT^+Sftpc^+ AT2 cells or tdT^+AGER^+ AT1 cells.

(F) A schematic diagram illustrating the experimental design.

(G) Immunostaining for tdT and Scgb1a1 on lung sections of *Scgb1a1-CreER;R26-tdT*, *Scgb1a1-CreER;R26-TLR*, and *Scgb1a1-CreER;R26-LZL-tdT* mice without tamoxifen treatment (left panel). Immunostaining for tdT and Sftpc on lung sections of *Scgb1a1-CreER;R26-tdT*, *Scgb1a1-CreER;R26-TLR*, and *Scgb1a1-CreER;R26-LZL-tdT* mice after tamoxifen treatment (right panel). The schematic diagrams (right side) shows the length of Stop cassette between the *loxP* sites of three genetic mice.

(H) Quantification of the percentage of $Scgb1a1^+$ cells expressing tdT of three genetic mice without tamoxifen treatment in (left panel). Quantification of the percentage of $Sftpc^+$ cells expressing tdT of three genetic mice after tamoxifen treatment in (right panel). Data are presented as mean \pm SD; n = 5 mice per group.

(I) A cartoon image showing that, using *Scgb1a1-CreER*, a subpopulation of AT2 cells was labeled by *R26-tdT* reporter, but very small number of AT2 cells were labeled by *R26-TLR* or *R26-NR2* reporters after tamoxifen treatment in these three genetic mice.

(J) A schematic diagram illustrating the experimental design.

(K) Immunostaining for tdT, ZsG, alveolar epithelial markers Sftpc, Lamp3, and AGER on lung sections of *Scgb1a1-CreER;Sftpc-DreER;R26-TLR* mice post-bleomycin injury showed that majority of the alveolar epithelium was labeled by tdT (upper panel). Immunostaining for tdT, ZsG, bronchiolar epithelial markers Krt5, Scgb1a1, and Ace-Tub on lung sections of *Scgb1a1-CreER;Sftpc-DreER;R26-TLR* mice post-bleomycin injury shows few bronchiolar epithelial type cells expressing tdT in the alveolar region (lower panel). White arrowheads, tdT^+Sftpc^+ AT2 cells, tdT^+Lamp3^+ AT2 cells, tdT^+AGER^+ AT1 cells, tdT^+Krt5^+ basal-like cells, $tdT^+Scgb1a1^+$ club-like cells or $tdT^+Ace-Tub^-$ cells.

(L) Quantification of the percentage of alveolar tdT^+ cells that express the markers of AT2 cells, AT1 cells, basal-like cells, club-like cells, and ciliated-like cells of *Scgb1a1-CreER;Sftpc-DreER;R26-TLR* mice post-bleomycin injury. Data are presented as mean \pm SD; n = 5 mice per group.

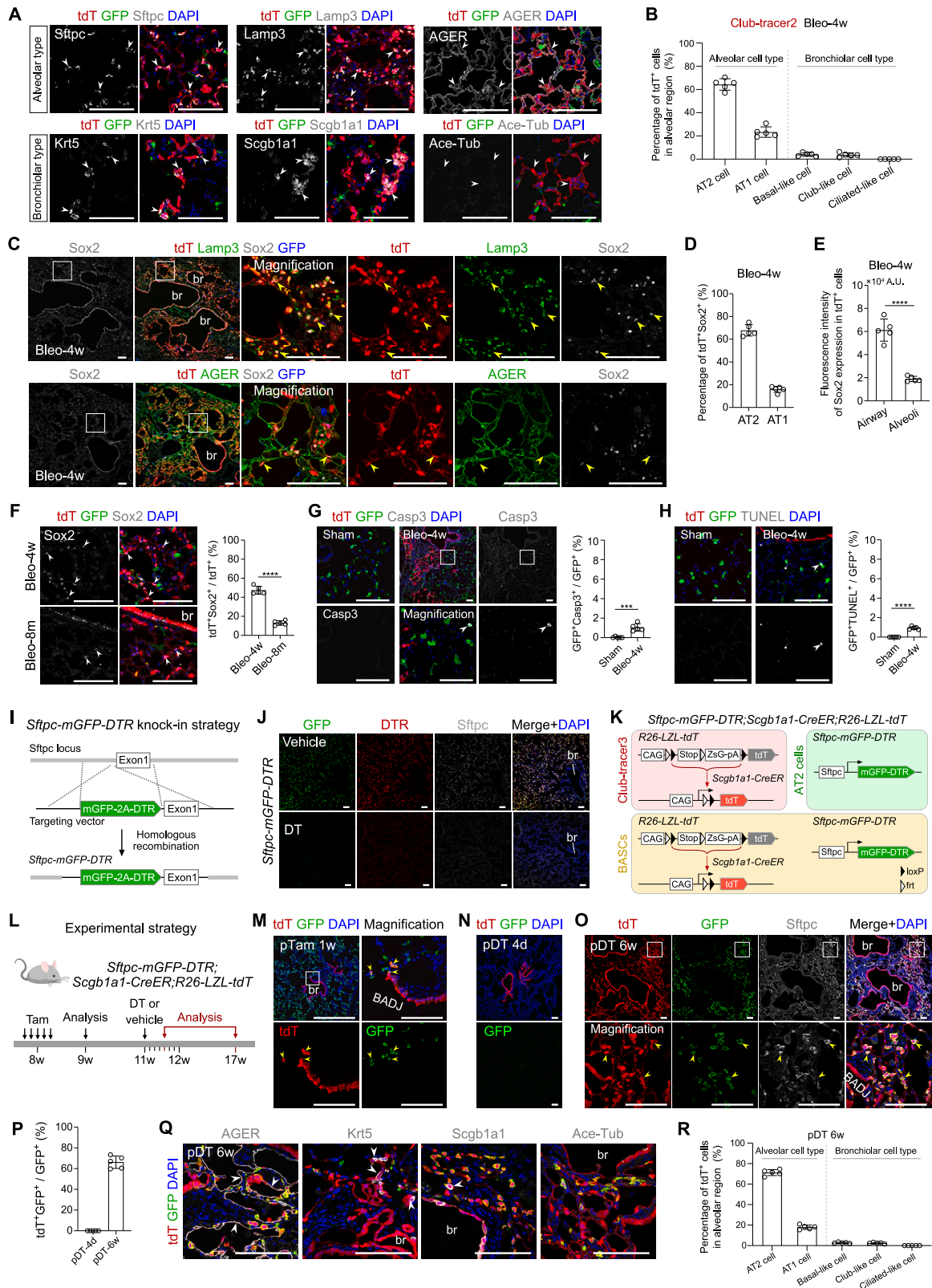
(M) A schematic diagram illustrating the experimental design.

(N) Immunostaining for tdT and Ki67 on the lung sections of *Sftpc-DreER;R26-rox-tdT* after 10 days bleomycin injury (upper panel). Yellow arrowheads, tdT^+Ki67^+ AT2 cells; White arrowheads, tdT^+AGER^+ AT1 cells. Immunostaining for GFP and Ki67 on the lung sections of *Sftpc-DreER;R26-rox-p21-GFP* after 10 days bleomycin injury (lower panel). White arrowheads, GFP^+AGER^+ AT1 cells.

(O) Quantification of the percentage of reporter⁺ cells expressing Ki67 in (N). Data are presented as mean \pm SD; n = 3 mice per group. ***p = 0.0005. Statistical analysis was performed by two-tailed unpaired Student's t test.

(P) Quantification of the percentage of reporter⁺ cells expressing AGER in (N). Data are presented as mean \pm SD; n = 3 mice per group. *p = 0.02. Statistical analysis was performed by two-tailed unpaired Student's t test.

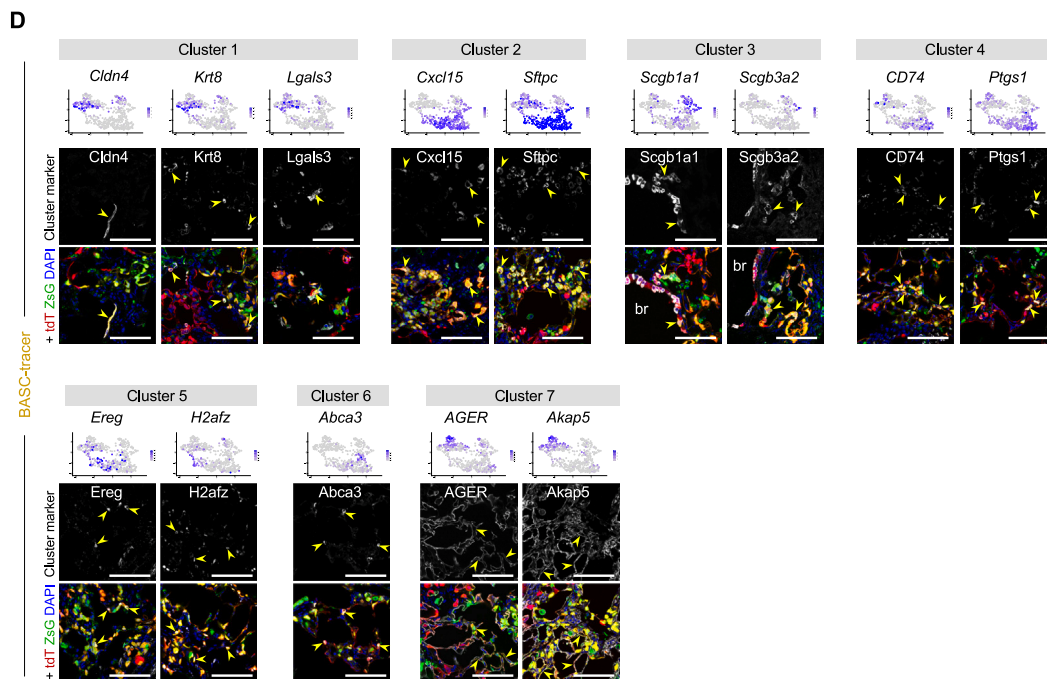
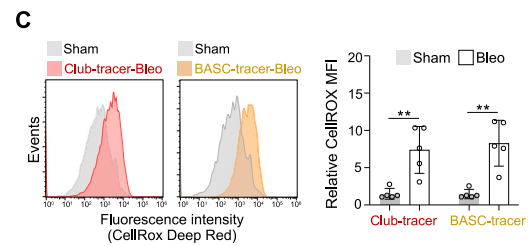
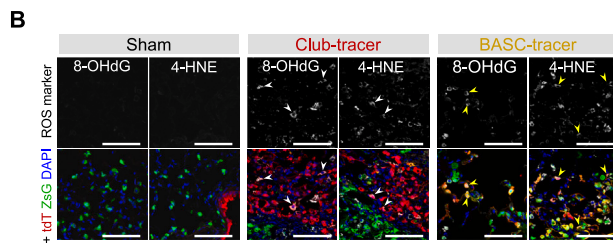
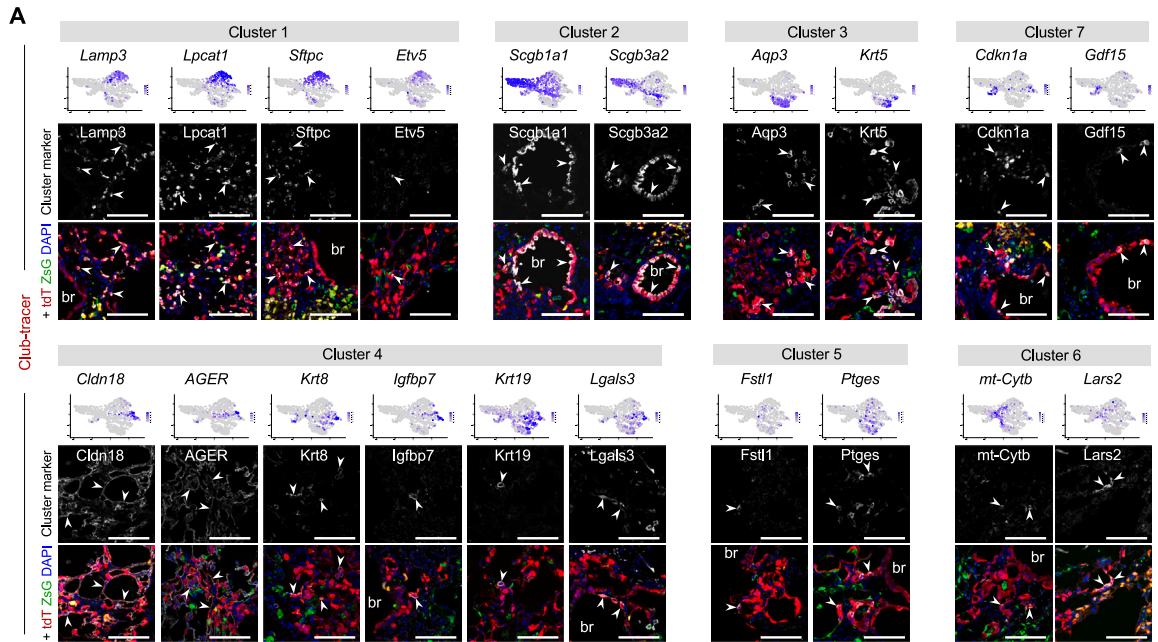
Tam, tamoxifen. tdT, tdTomato. ZsG, ZsGreen. Bleo, bleomycin. Ace-Tub, acetylated-tubulin. Data are presented as mean \pm SD; n = 3–5 mice per group. Scale bars, 100 μ m.



(legend on next page)

Figure S5. Club progenitors regenerate alveoli in p21 and bleomycin- and DT-induced lung-injury models, related to Figure 5

- (A) Immunostaining for tdT, GFP, alveolar epithelial markers Sftpc, Lamp3, and AGER on lung sections of *Scgb1a1-CreER;Sftpc-DreER;R26-rox-p21-GFP;R26-LZL-tdT* mice at 4 weeks post-bleomycin injury (upper panel). Immunostaining for tdT, ZsG, bronchiolar epithelial markers Krt5, Scgb1a1, and Ace-Tub on lung sections of *Scgb1a1-CreER;Sftpc-DreER;R26-rox-p21-GFP;R26-LZL-tdT* mice at 4 weeks post-bleomycin injury (lower panel). White arrowheads, tdT⁺Sftpc⁺ AT2 cells, tdT⁺Lamp3⁺ AT2 cells, tdT⁺AGER⁺ AT1 cells, tdT⁺Krt5⁺ basal-like cells, tdT⁺Scgb1a1⁺ club-like cells or tdT⁺Ace-Tub⁺ cells.
- (B) Quantification of the percentage of alveolar tdT⁺ cells that express the markers of AT2 cells, AT1 cells, basal-like cells, club-like cells, and ciliated-like cells of *Scgb1a1-CreER;Sftpc-DreER;R26-rox-p21-GFP;R26-LZL-tdT* mice at 4 weeks post-bleomycin injury. Data are presented as mean ± SD; n = 5 mice per group.
- (C) Immunostaining for tdT, GFP, Sox2, alveolar epithelial markers Lamp3 and AGER on lung sections of *Scgb1a1-CreER;Sftpc-DreER;R26-rox-p21-GFP;R26-LZL-tdT* mice at 4 weeks post-bleomycin injury. Yellow arrowheads, tdT⁺GFP⁺Sox2⁺Lamp3⁺ AT2 cells (upper panel), or tdT⁺GFP⁺Sox2⁺AGER⁺ AT2 cells (lower panel).
- (D) Quantification of the percentage of alveolar tdT⁺Sox2⁺ cells expressing AT2 marker Lamp3 and AT1 marker AGER after bleomycin injury in (C). Data are presented as mean ± SD; n = 5 mice per group.
- (E) Quantification of the fluorescence intensity of Sox2 expression in the airway and alveolar tdT⁺ cells of the *Scgb1a1-CreER;Sftpc-DreER;R26-rox-p21-GFP;R26-LZL-tdT* mice after bleomycin injury. Data are presented as mean ± SD; n = 5 mice per group.
- (F) Immunostaining for tdT, GFP, and Sox2 on lung sections of *Scgb1a1-CreER;Sftpc-DreER;R26-rox-p21-GFP;R26-LZL-tdT* mice at 4 weeks and 8 months post-bleomycin injury (left panel). White arrowheads, tdT⁺GFP⁺Sox2⁺ cells. Quantification of the percentage of alveolar tdT⁺ cells expressing Sox2 on lung sections at 4 weeks and 8 months post-bleomycin injury (right panel). Data are presented as mean ± SD; n = 5 mice per group.
- (G) Immunostaining for tdT, GFP, and cleaved caspase-3 (Casp3) on lung sections of *Scgb1a1-CreER;Sftpc-DreER;R26-rox-p21-GFP;R26-LZL-tdT* mice at 4 weeks post-bleomycin injury or sham (PBS) treatment (left panel). White arrowheads, tdT⁺GFP⁺Casp3⁺ cells. Quantification of the percentage of GFP⁺ cells expressing Casp3 at 4 weeks post-bleomycin or sham treatment (right panel). Data are presented as mean ± SD; n = 5 mice per group. ****p = 0.0004. *p* value was calculated by unpaired two-sided Student's *t* test.
- (H) Immunostaining for tdT, GFP, and TUNEL on lung sections of *Scgb1a1-CreER;Sftpc-DreER;R26-rox-p21-GFP;R26-LZL-tdT* mice at 4 weeks post-bleomycin injury or sham (PBS) treatment (left panel). White arrowheads, tdT⁺GFP⁺TUNEL⁺ cells. Quantification of the percentage of GFP⁺ cells labeled by TUNEL at 4 weeks post-bleomycin or sham treatment (right panel). Data are presented as mean ± SD; n = 5 mice per group. ****p < 0.0001. *p* value was calculated by unpaired two-sided Student's *t* test.
- (I) A schematic diagram illustrating the generation of *Sftpc-mGFP-DTR* line by knocking the mGFP-2A-DTR sequence into the 5' UTR of the endogenous *Sftpc* gene locus via homologous recombination. DTR is the diphtheria toxin (DT) receptor, and this line can be used for deleting *Sftpc*⁺ cells by DT treatment.
- (J) Immunostaining for GFP, DTR, and *Sftpc* on lung sections of *Sftpc-mGFP-DTR* mice at 4 days (4d) post-DT or vehicle (PBS) treatment.
- (K) A schematic diagram illustrating the genetic strategy for targeting of club cells, BASCs, and AT2 cells by using *Sftpc-mGFP-DTR;Scgb1a1-CreER;R26-LZL-tdT* mice. Theoretically, in this triple positive line, Scgb1a1⁺Sftpc⁺ club cells (Club-tracer3) were traced by tdT, Scgb1a1⁺Sftpc⁺ BASCs were labeled by both tdT and GFP, and Scgb1a1⁺Sftpc⁺ AT2 cells were labeled by GFP. Both BASCs and AT2 cells express DTR.
- (L) A schematic diagram illustrating the experimental design for tamoxifen, DT, or vehicle (PBS) treatment, and tissue analysis. DT was treated through tracheal instillation.
- (M) Immunostaining for tdT and GFP on lung sections of *Sftpc-mGFP-DTR;Scgb1a1-CreER;R26-LZL-tdT* mice at 1 week (w) post tamoxifen (pTam) treatment. Yellow arrowheads, tdT⁺GFP⁺ BASCs.
- (N) Immunostaining for tdT and GFP on lung sections of *Sftpc-mGFP-DTR;Scgb1a1-CreER;R26-LZL-tdT* mice at 4 days post-DT (pDT) treatment.
- (O) Immunostaining for tdT, GFP, and *Sftpc* on lung sections of *Sftpc-mGFP-DTR;Scgb1a1-CreER;R26-LZL-tdT* mice at 6 weeks post-DT treatment. Yellow arrowheads, tdT⁺GFP⁺Sftpc⁺ AT2 cells.
- (P) Quantification of the percentage of GFP⁺ cells expressing tdT at 4 days and 6 weeks post-DT injury. Data are presented as mean ± SD; n = 5 mice per group.
- (Q) Immunostaining for tdT, GFP, AGER, Krt5, Scgb1a1, or Ace-Tub on lung sections of *Sftpc-mGFP-DTR;Scgb1a1-CreER;R26-LZL-tdT* mice at 6 weeks post-DT treatment. White arrowheads, tdT⁺AGER⁺ AT1 cells, tdT⁺Krt5⁺ basal-like cells or tdT⁺Scgb1a1⁺ club-like cells.
- (R) Quantification of the percentage of alveolar tdT⁺ cells that express the markers of AT2 cells, AT1 cells, basal-like cells, club-like cells, and ciliated-like cells of *Sftpc-mGFP-DTR;Scgb1a1-CreER;R26-LZL-tdT* mice at 6 weeks post-DT treatment. Data are presented as mean ± SD; n = 5 mice per group. Data are presented as mean ± SD; n = 5 mice per group. Scale bars, 100 μm. BADI, alveolar-duct junctions.



(legend on next page)

Figure S6. Characterization of the cell cluster markers from single cell analysis, related to Figure 6

(A) Immunostaining for tdT, ZsG with cell cluster markers of Club-tracer on lung sections of *Scgb1a1-CreER;Sftpc-DreER;R26-TLR* mice at 4 weeks after bleomycin injury. Cluster 1 markers stained were Lamp3, Lpcat1, Sftpc, and Etv5. Cluster 2 markers stained were Scgb1a1 and Scgb3a2. Cluster 3 markers stained were Aqp3 and Krt5. Cluster 4 markers stained were Cldn18, AGER, Krt18, Igfbp7, Krt19, and Lgals3. Cluster 5 markers stained were Fstl1 and Ptgs. Cluster 6 markers stained were mt-Cytb and Lars2. Cluster 7 markers stained were Cdkn1a and Gdf15. White arrowheads indicated the tdT⁺ZsG⁻ cells (Club-tracer) expressing the above cluster markers.

(B) Immunostaining for tdT, ZsG, 8-Hydroxy-2'-deoxyguanosine (8-OHdG), and 4-hydroxynonenal (4-HNE) on lung sections of *Scgb1a1-CreER;Sftpc-DreER;R26-TLR* mice at 4 weeks after bleomycin or sham (PBS) treatment. No 8-OHdG and 4-HNE signals were detected on lung sections of the sham group (left panel) while detected on the bleomycin group (middle and right panels). White arrowheads, tdT⁺ZsG⁻8-OHdG⁺ cells or tdT⁺ZsG⁻4-HNE⁺ cells. Yellow arrowheads, tdT⁺ZsG⁺8-OHdG⁺ cells or tdT⁺ZsG⁺4-HNE⁺ cells.

(C) Quantitative cytofluorimetric analysis of the intracellular ROS production within Club-tracer and BASC-tracer of *Scgb1a1-CreER;Sftpc-DreER;R26-TLR* mice at 4 weeks after bleomycin (Bleo) or sham (PBS) treatment. The cells of ROS production were detected by staining with CellROX-Deep Red reagent and then subjected to FACS analysis. The flow cytometry results showed that the fluorescence intensity of Club-tracer and BASC-tracer cell populations shifted to the right in bleomycin-injured group compared to the sham group (left panel). Quantification of the relative mean fluorescence intensity (MFI) of ROS production within Club-tracer and BASC-tracer of bleomycin group compared to sham treatment (right panel). Data are presented as mean ± SD; n = 5 mice per group. Club-tracer: bleomycin versus sham, **p = 0.0035; BASC-tracer: bleomycin versus sham, ***p = 0.0012; Statistical analysis was performed by two-tailed unpaired Student's t test.

(D) Immunostaining for tdT, ZsG with cluster markers of BASC-tracer on lung sections of *Scgb1a1-CreER;Sftpc-wDreER;R26-TLR* mice at 4 weeks after bleomycin injury. Cluster 2 markers stained were Cldn4, Krt8, and Lgals3. Cluster 2 markers stained were Cxcl15 and Sftpc. Cluster 3 markers stained were Scgb1a1 and Scgb3a2. Cluster 4 markers stained were CD74 and Ptgs1. Cluster 5 markers stained were Ereg and H2afz. Cluster 6 marker stained was Abca3. Cluster 7 markers stained were AGER and Akap5. Yellow arrowheads indicated the tdT⁺ZsG⁺ cells (BASC-tracer) expressing the above cluster markers. Data are presented as mean ± SD; n = 5 mice per group. Scale bars, 100 μm.

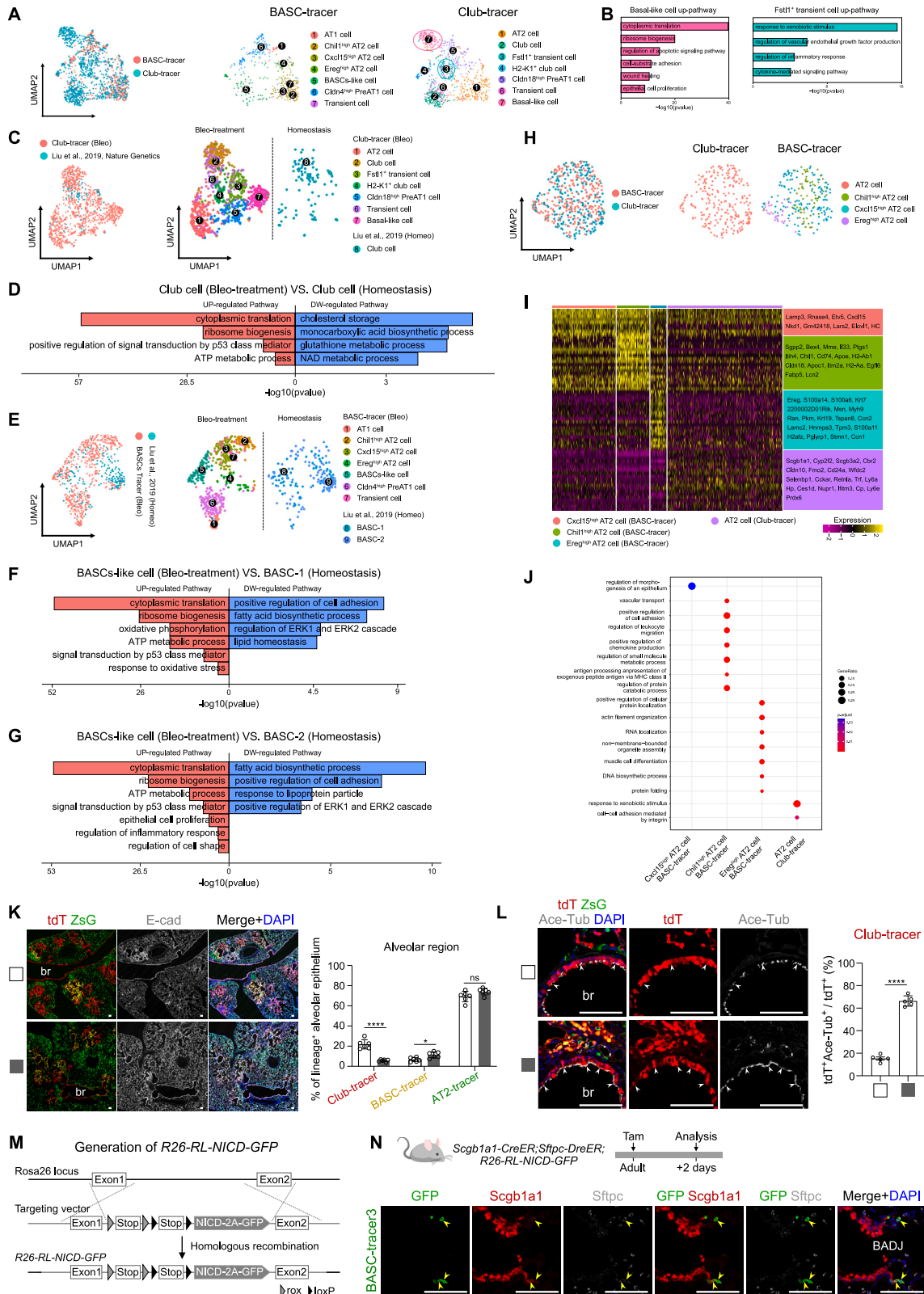


Figure S7. scRNA-seq analysis of cells from Club-tracer, BASC-tracer, and AT2-tracer after injury, related to Figures 6 and 7

(A) The plots depict the UMAP embedding of cells from the integration of Club-tracer and BASC-tracer objects.

(B) The bar graph shows the significantly enriched GO pathways in upregulated differential expression genes (DEGs) in Trp63⁺ cells (left) or Fst11⁺ cells (right) compared to the remaining cells. DEGs were chosen with a log₂(FC ratio) above 0.5 and an adjusted p value below 0.01. The significance threshold for enriched GO pathways was set at a p value below 0.05.

(C) The plots visualize the UMAP embedding of integrated club cells from the Club-tracer and Liu et al., 2019.

(D) The bar graph shows the enriched GO pathways in upregulated (left) and downregulated (right) DEGs of club cells of Club-tracer (bleo-treatment) compared to club cells of Liu et al., 2019 (homeostasis). DEGs were chosen with a log₂(FC ratio) above 1 and an adjusted p value below 0.05. The significance threshold for enriched GO pathways was set at a p value below 0.05.

(E) The plots visualize the UMAP embedding of integrated BASCs-like cells from the BASC-tracer and BASCs from Liu et al., 2019.

(F and G) The bar graph shows the enriched GO pathways in upregulated (left) and downregulated (right) DEGs of BASCs-like cells of BASC-tracer (bleo-treatment) compared to BASC-1 (F) and BASC-2 (G) of Liu et al., 2019 (homeostasis). DEGs were chosen with a log₂(FC ratio) above 1 and an adjusted p value below 0.05. The significance threshold for enriched GO pathways was set at a p value below 0.05.

(H) The plots visualize the UMAP embedding of integrated AT2 cells from Club-tracer and BASC-tracer.

(I and J) The heatmap (I) shows the top 20 DEGs (or all DEGs, if fewer than 20) between the AT2 cell subpopulation from BASC-tracer and from Club-tracer. DEGs were chosen with a log₂(FC ratio) above 0.5 and an adjusted p value below 0.01. The dotplot (J) shows the significantly enriched GO pathways in all DEGs across different cell subpopulations described in (I) respectively. The significance threshold for enriched GO pathways was set at a p value below 0.05.

(K) Immunostaining for tdT, ZsG, and E-cad on lung sections of *Scgb1a1-CreER;Sftpc-DreER;R26-TLR;Rbpj^{fllox/+}* control mice (left upper panel) and *Scgb1a1-CreER;Sftpc-DreER;R26-TLR;Rbpj^{fllox/fllox}* mutant mice (left lower panel) at 4 weeks after bleomycin injury. Quantification of the percentage of alveolar E-cad⁺ cells that were labeled by Club-tracer, BASC-tracer, or AT2-tracer after bleomycin injury in control and mutant groups (right panel). Data are presented as mean ± SD; n = 5 mice per group. Club-tracer: bleomycin versus sham, ****p < 0.0001; BASC-tracer: bleomycin versus sham, **p = 0.0108; AT2-tracer: bleomycin versus sham, p = 0.0841; ns, non-significant. Statistical analysis was performed by a two-tailed unpaired Student's t test.

(L) Immunostaining for tdT, ZsG, and Ace-Tub on lung sections of the control and mutant group mice after bleomycin injury (left panel). White arrowheads, tdT⁺Ace-Tub⁺ ciliated cells. Quantification of the percentage of club-tracer expressing Ace-Tub in bronchioles (right panel). Data are presented as mean ± SD; n = 5 mice per group. ****p < 0.0001. p value was calculated by unpaired two-sided Student's t test.

(M) A schematic diagram illustrating the knock-in strategy of *R26-RL-NICD-GFP* line by homologous recombination using CRISPR/cas9.

(N) A schematic diagram illustrating the experimental design (upper panel). Immunostaining for GFP, Scgb1a1, and Sftpc on lung sections of *Scgb1a1-CreER;Sftpc-DreER;R26-RL-NICD-GFP* after tamoxifen treatment (lower panel). Yellow arrowheads, GFP⁺Scgb1a1⁺Sftpc⁺ BASCs. Data are presented as mean ± SD; n = 5–6 mice per group. Scale bars, 100 μm.